Terascale Physics Opportunities at a High Statistics, High Energy Neutrino Scattering Experiment: NuSOnG

T. Adams[5], P. Batra[3], L. Bugel[3], L. Camilleri[3], J.M. Conrad[3], A. de Gouvêa[11], P.H. Fisher[8], J.A. Formaggio[8], J. Jenkins[11], G. Karagiorgi[3], T.R. Kobilarcik[4], S. Kopp[15], G. Kyle[10], W.A. Loinaz[1], D.A. Mason[4], R. Milner[8], R. Moore[4], J. G. Morfín[4], M. Nakamura[9], D. Naples[12], P. Nienaber[13], F.I Olness[14], J.F. Owens[5], S.F. Pate[10], A. Pronin[16], W.G. Seligman[3], M.H. Shaevitz[3], H. Schellman[11], I. Schienbein[7], M.J. Syphers[4], T.M.P. Tait[2,11], T. Takeuchi[16], C.Y. Tan[4], R.G. Van de Water[6], R.K. Yamamoto[8], J.Y. Yu[14]

[1] *Amherst College, Amherst, MA 01002*
[2] *Argonne National Laboratory, Argonne , IL 60439*
[3] *Columbia University, New York, NY 10027*
[4] *Fermi National Accelerator Laboratory, Batavia IL 60510*
[5] *Florida State University, Tallahassee, FL 32306*
[6] *Los Alamos National Accelerator Laboratory, Los Alamos, NM 87545*
[7] *LPSC, Université Joseph Fourier Grenoble 1, 38026 Grenoble, France*
[8] *Massachusetts Institute of Technology, Cambridge, MA 02139*
[9] *Nagoya University, 464-01, Nagoya, Japan*
[10] *New Mexico State University, Las Cruces, NM 88003*
[11] *Northwestern University, Evanston, IL 60208*
[12] *University of Pittsburgh, Pittsburgh, PA 15260*
[13] *Saint Mary's University of Minnesota, Winona, MN 55987*
[14] *Southern Methodist University, Dallas, TX 75205*
[15] *University of Texas, Austin TX 78712*
[16] *Virginia Tech, Blacksburg VA 24061*

(Dated: March 12, 2008)

This article presents the physics case for a new high-energy, ultra-high statistics neutrino scattering experiment, NuSOnG (Neutrino Scattering on Glass). This experiment uses a Tevatron-based neutrino beam to obtain over an order of magnitude higher statistics than presently available for the purely weak processes $\nu_\mu + e^- \to \nu_\mu + e^-$ and $\nu_\mu + e^- \to \nu_e + \mu^-$. A sample of Deep Inelastic Scattering events which is over two orders of magnitude larger than past samples will also be obtained. As a result, NuSOnG will be unique among present and planned experiments for its ability to probe neutrino couplings to Beyond the Standard Model physics. Many Beyond Standard Model theories physics predict a rich hierarchy of TeV-scale new states that can correct neutrino cross-sections, through modifications of $Z\nu\nu$ couplings, tree-level exchanges of new particles such as Z's, or through loop-level oblique corrections to gauge boson propagators. These corrections are generic in theories of extra dimensions, extended gauge symmetries, supersymmetry, and more. The sensitivity of NuSOnG to this new physics extends beyond 5 TeV mass scales. This article reviews these physics opportunities.

I. INTRODUCTION

Exploring for new physics at the "Terascale" – energy scales of ~ 1 TeV and beyond – is the highest priority for particle physics. A new, high energy, high statistics neutrino scattering experiment running at the Tevatron at Fermi National Accelerator Laboratory can look beyond the Standard Model at Terascale energies by making precision electroweak measurements, direct searches for novel phenomena, and precision QCD studies. In this article we limit the QCD discussion to those topics which directly support the exploration of the Terascale; there are additional QCD studies that may be done and these will be covered in a future publication. The ideas developed in this article were proposed within the context of an expression of interest for a new neutrino experiment, NuSOnG (Neutrino Scattering On Glass) [1].

A unique and important measurement of the NuSOnG physics program is the ratio of neutral current (NC) and charged current (CC) neutrino-electron scattering, which probes new physics. The leading order Feynman diagrams for these processes are shown in Fig. 1. The NC process, $\nu_\mu + e^- \to \nu_\mu + e^-$, called "elastic scattering" or ES, provides the sensitivity to the Terascale physics. This process can explore new physics signatures in the neutrino sector which are not open to other, presently planned experiments. The CC process, called "inverse muon decay" or IMD, $\nu_\mu + e^- \to \nu_e + \mu^-$, is well understood in the Standard Model due to precision measurement of muon decay [2]. Since the data samples are

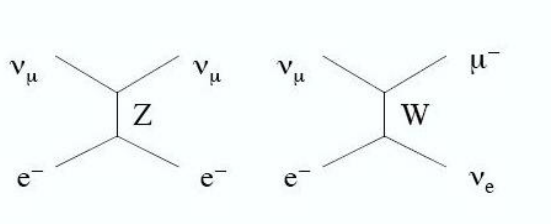

FIG. 1: Left: "elastic scattering" (ES). Right: "Inverse Muon Decay" (IMD).

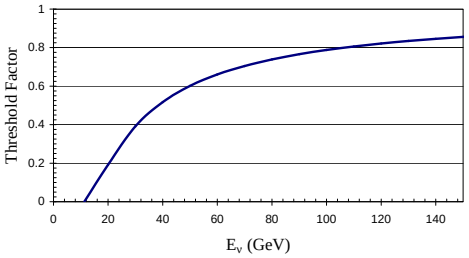

FIG. 2: Threshold factor for the IMD cross section, as a function of neutrino energy.

collected with the same beam, target and detector at the same time, the ratio of ES to IMD events cancels many systematic errors while maintaining a strong sensitivity to the physics of interest. Our measurement goal of the ES to IMD ratio is a 0.7% error, adding systematic and statistical errors in quadrature. The high sensitivity which we propose arises from the combined high energy and high intensity of the NuSOnG design, leading to event samples more than an order of magnitude higher than past experiments.

Normalizing the ES to the IMD events represents an important step forward from past ES measurements, which have normalized neutrino-mode ES measurements to the antineutrino mode, $\bar{\nu}_\mu + e^- \to \bar{\nu}_\mu + e^-$[3, 4]. The improvement is in both the experimental and the theoretical aspects of the measurement. First, the flux contributing to IMD and ν ES is identical, whereas neutrino and antineutrino fluxes are never identical and so require corrections. Second, the ratio of ν ES to $\bar{\nu}$ ES cancels sensitivity to Beyond Standard Model (BSM) physics effects from the NC to CC coupling ratio, ρ, which are among the primary physics goals of the NuSOnG measurement. In contrast, there is no such cancellation in the ES to IMD ratio.

The design of this experiment, described in Sec. II, is driven both by requiring sufficient statistics to make precision neutrino-electron scattering measurements and by the need for a neutrino flux which does not extend below the IMD threshold. The threshold for IMD events is

$$E_\nu \geq E_\mu \geq \frac{m_\mu^2}{2m_e} = 10.9 \text{ GeV}, \qquad (1)$$

where we have dropped the small m_e^2 term for simplicity. The functional form above threshold, shown in Fig. 2, is given by $(1 - m_\mu^2/E_{cm}^2)^2$, where E_{cm} is the center of mass energy. Thus a high energy neutrino beam is required to obtain a high statistics sample of these events. The flux design should provide a lower limit on the beam energy of about 30 GeV, still well above the IMD threshold.

Sec. III describes the Standard Model Physics of neutrino electroweak scattering, for both electron and quark targets. In this section, the value of the normalization of the ES to IMD events is further explored. The very high statistics will also permit an electroweak measurement using the deep inelastic scattering (DIS) data sample from NuSOnG, via the "Paschos Wolfenstein method" (PW) [5]. The best electroweak measurement using DIS events to date comes from the NuTeV experiment, which has observed an anomaly. The status of this result is reviewed below. Making conservative assumptions concerning systematic improvements over NuTeV, our measurement goal using this technique is a 0.4% error on $\sin^2\theta_W$, adding statistical and systematic errors in quadrature.

In Sec. IV, we discuss NuSOnG's potential to discover or constrain new physics through indirect probes, by making precision measurements of SM processes to look for deviations from SM predictions. We first frame the issue by considering in turn several model-independent parameterizations of possible new physics and asking what constraints will be imposed on new physics in the event NuSOnG agrees with the SM. (1) Oblique correction parameters describe the effects of heavy new states in vector boson loops. (2) New states may induce higher-dimensional effective operators involving neutrinos. Finally, (3) new states may modify the couplings of the gauge bosons to neutrinos and leptons, including possibly violating lepton universality. In each case we consider the ability of NuSOnG to detect or constrain these types of deviations from the SM.

In Sec. V, we examine specific models for new physics. We begin by presenting the sensitivity to a set of new physics models. In particular, we consider

- typical Z' models,
- non-degenerate leptoquark models,
- R-parity violating SUSY models,
- extended Higgs models.

The models were selected because they are often used as benchmarks in the literature. While this list is not exhaustive, it serves to illustrate the possibilities. For each case, we consider how NuSOnG compares to other measurements and note the unique contributions. We end this section by approaching the question from the opposite view, asking: how could the results from NuSOnG

clarify the underlying physics model, should evidence of new physics emerge from LHC in the near future?

The very large ($\sim$ 600 million event) DIS sample will allow the opportunity for precision studies of QCD. There are many interesting measurements which can be made in their own right, and these will be the topic of a future paper. Given the theme of this article, instead, in Sec. VI, we concentrate on those QCD measurements that are important to NuSOnG's Terascale physics program. We also note that there is a set of outside measurements that bear on suggested solutions to the NuTeV anomaly and which will be incorporated into the NuSOnG analysis.

Lastly, in Sec. VII we observe that the very high flux which is necessary for the indirect searches permits complementary direct searches for new physics. A wide range of searches can be done, and we limit this discussion to those topics related and complementary to the indirect Terascale studies. We specifically consider searches for evidence of:

- non-unitarity in the light neutrino mixing matrix;
- wrong-sign inverse muon decay (WSIMD), $\bar{\nu}_\mu + e^- \to \mu^- + \bar{\nu}_e$;
- decays of neutrissimos, *i.e.,* moderately-heavy neutral-heavy-leptons, with masses above 45 GeV.

II. CONCEPTUAL DESIGN FOR THE EXPERIMENT

In order to discuss the physics case for a new high energy, high statistics experiment, one must specify certain design parameters for the beam and detector. The beam and detector should marry the best aspects of NuTeV [6], the highest energy neutrino experiment, and Charm II [8], the experiment with the largest ES sample to date. The plan presented here is not optimized, but provides a basis for discussion. The final design of the NuSOnG detector will be based on these concepts, and is still under development.

In this section, we present, but do not justify, the design choices. Later in this article, we discuss the reasoning for the choices, particularly in Secs. III C and III D.

We will assume a beam design based on the one used by the NuTeV experiment [6], which is the most recent high energy neutrino experiment. This experiment used 800 GeV protons on target. The beam flux, shown in Fig. 3, is ideal for the physics case for several reasons. There is essentially no flux below 30 GeV, hence all neutrinos are well above the IMD threshold. It is sign-selected: in neutrino mode, 98.2% of neutrino interactions were due to π^+ and K^+ secondaries, while in antineutrino mode 97.3% came from π^- and K^-. The "wrong sign" content was very low, with a 0.03% antineutrino contamination in neutrino mode and 0.4% neutrino contamination in antineutrino mode. The electron-flavor content was 1.8% in neutrino mode and 2.3% in antineutrino mode. The

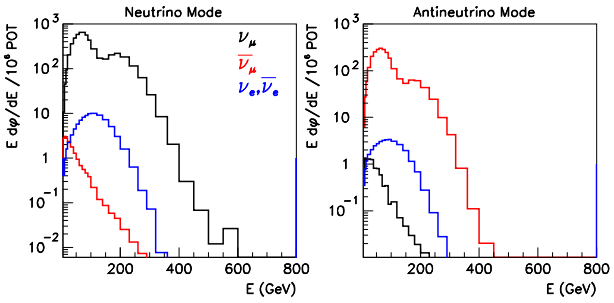

FIG. 3: The assumed energy-weighted flux, from the NuTeV Experiment [6], in neutrino mode (left) and antineutrino mode (right). Black: muon neutrino, red: muon antineutrino, blue: electron neutrino and antineutrino flux.

major source of these neutrinos is $K^\pm_{e3}$ decay, representing 1.7% of the total flux in neutrino mode, and 1.6% in antineutrino mode.

Redesign of the beamline for NuSOnG is expected to lead to modest changes in these ratios. For example, if the decay pipe length is 1.5 km rather than 440 m, as in NuTeV, the π/K ratio increases by 20% and the fractional ν_e content is reduced.

With respect to Tevatron running conditions, we will assume that twenty times more protons on target (POT) per year can be produced for NuSOnG compared to NuTeV. This is achieved through three times higher intensity per pulse (or "ping"). Nearly an order of magnitude more pulses per spill are provided. Our studies assume 4×10^{19} POT/year, with 5 years of running. Preliminary studies supporting these goals are provided in reference [7].

The event rates quoted below are consistent with $1.5{\times}10^{20}$ protons on target in neutrino running and 0.5×10^{20} protons on target in antineutrino running. The choice to emphasize neutrino running is driven by obtaining high statistics ES, which has a higher cross section for neutrino scatters, and to use the IMD for normalization – this process only occurs in neutrino scattering. The Standard Model forbids an IMD signal in antineutrino mode. However, some antineutrino running is required for the physics described in the following sections, especially the PW electroweak measurement.

The beam from such a design is highly forward directed. NuTeV was designed so that 90% of the neutrinos from pion decay were contained within the detector face, where the detector was located at 1 km. For NuSOnG, which will use a 5 m detector, $\sim$90% of the neutrinos from pion decay are contained at $\sim$3 km.

The optimal detector is a fine-grained calorimeter for electromagnetic shower reconstruction followed by a toroid muon spectrometer. This allows excellent reconstruction of the energy of the outgoing lepton from charged current events. We employ a Charm II style design [8], which uses a glass target calorimeter followed by a toroid. We assume one inch glass panels with ac-

600M	ν_μ CC Deep Inelastic Scattering
190M	ν_μ NC Deep Inelastic Scattering
75k	ν_μ electron NC elastic scatters (ES)
700k	ν_μ electron CC quasi-elastic scatters (IMD)
33M	$\bar{\nu}_\mu$ CC Deep Inelastic Scattering
12M	$\bar{\nu}_\mu$ NC Deep Inelastic Scattering
7k	$\bar{\nu}_\mu$ electron NC elastic scatters (ES)
0k	$\bar{\nu}_\mu$ electron CC quasi-elastic scatters (WSIMD)

TABLE I: Rates assumed for this paper. NC indicates "neutral current" and CC indicates "charged current."

tive detectors interspersed for energy and position measurement. Glass provides an optimal choice of density, low enough to allow electromagnetic showers to be well sampled, but high enough that the detector length does not compromise acceptance for large angle muons by the toroid. Approximately 10% of the glass will be doped with scintillator to allow for background studies, as discussed in Sec. III D.

The design introduces four identical sub-detectors of this glass-calorimeter and toroid design, each a total of 29 m in length (including the toroid). Between each sub-detector is a 15 m decay region for direct searches for new physics. The total fiducial volume is 3 ktons.

The NuSOnG run plan, for reasons discussed in Sec. III B and III C, concentrates on running in neutrino mode. This design will yield the rates shown in Table I. These rates, before cuts, are assumed throughout the rest of the discussion. We can compare this sample to past experiments. The present highest statistics sample for ν_μ and $\bar{\nu}_\mu$ ES is from CHARM II, with 2677±82 events in neutrino mode and 2752±88 events in antineutrino mode [4]. Thus the proposed experiment will have a factor of 30 (2.5) more $\nu(\bar{\nu})$-electron events. As an example, after cuts, the first method of analysis described in Sec. III D retains 63% of the ν sample. For deep inelastic scattering, 600M and 190M events are expected in neutrino and antineutrino modes, respectively. After minimal cuts to isolate DIS events [9], NuTeV had 1.62M DIS (NC+CC) events in neutrino mode and 0.35M in antineutrino mode; thus NuSOnG has orders of magnitude more events.

The detector may also incorporate several specialized regions. A region of fine vertex-tracking would facilitate measurements for the electroweak analysis, as described in Sec. VI C. Two possibilities are under consideration: an emulsion detector or a silicon detector of the style of NOMAD-STAR [10]. Both are compact and easily accommodated. For QCD studies, which are beyond the scope of this paper, it will also be useful to intersperse alternative target materials: C, Al, Fe, and Pb.

III. ELECTROWEAK MEASUREMENTS IN NEUTRINO SCATTERING

Neutrino neutral current (NC) scattering is an ideal probe for new physics. An experiment like NuSOnG is unique in its ability to test the NC couplings by studying scattering of neutrinos from both electrons and quarks. A deviation from the Standard Model predictions in both the electron and quark measurements would present a compelling case for new physics.

The exchange of the Z boson between the neutrino ν and fermion f leads to the effective interaction:

$$\begin{aligned}\mathcal{L} &= -\sqrt{2}G_F\Big[\,\bar{\nu}\gamma_\mu\big(g_V^\nu - g_A^\nu\gamma_5\big)\nu\,\Big]\Big[\,\bar{f}\gamma^\mu\big(g_V^f - g_A^f\gamma_5\big)f\,\Big] \\ &= -\sqrt{2}G_F\Big[\,g_L^\nu\,\bar{\nu}\gamma_\mu(1-\gamma_5)\nu + g_R^\nu\,\bar{\nu}\gamma_\mu(1+\gamma_5)\nu\,\Big] \\ &\qquad \times\Big[\,g_L^f\,\bar{f}\gamma^\mu(1-\gamma_5)f + g_R^f\,\bar{f}\gamma^\mu(1+\gamma_5)f\,\Big]\,, \end{aligned} \tag{2}$$

where the Standard Model values of the couplings are:

$$\begin{aligned} g_L^\nu &= \sqrt{\rho}\left(+\frac{1}{2}\right)\,, \\ g_R^\nu &= 0\,, \\ g_L^f &= \sqrt{\rho}\left(I_3^f - Q^f\sin^2\theta_W\right)\,, \\ g_R^f &= \sqrt{\rho}\left(-Q^f\sin^2\theta_W\right)\,, \end{aligned} \tag{3}$$

or equivalently,

$$\begin{aligned} g_V^\nu &= g_L^\nu + g_R^\nu = \sqrt{\rho}\left(+\frac{1}{2}\right)\,, \\ g_A^\nu &= g_L^\nu - g_R^\nu = \sqrt{\rho}\left(+\frac{1}{2}\right)\,, \\ g_V^f &= g_L^f + g_R^f = \sqrt{\rho}\left(I_3^f - 2Q^f\sin^2\theta_W\right)\,, \\ g_A^f &= g_L^f - g_R^f = \sqrt{\rho}\left(I_3^f\right)\,. \end{aligned} \tag{4}$$

Here, I_3^f and Q^f are the weak isospin and electromagnetic charge of fermion f, respectively. In these formulas, ρ is the relative coupling strength of the neutral to charged current interactions ($\rho = 1$ at tree level in the Standard Model). The weak mixing parameter, $\sin^2\theta_W$, is related (at tree level) to G_F, M_Z and α by

$$\sin^2 2\theta_W = \frac{4\pi\alpha}{\sqrt{2}G_F M_Z^2}. \tag{5}$$

A. Neutrino Electron Elastic Scattering

The differential cross section for ν_μ and $\bar{\nu}_\mu$ ES, defined using the coupling constants described above, is:

$$\begin{aligned}\frac{d\sigma}{dT} &= \frac{2G_F^2 m_e}{\pi}\Bigg[(g_L^\nu g_V^e \pm g_L^\nu g_A^e)^2 \\ &\qquad +(g_L^\nu g_V^e \mp g_L^\nu g_A^e)^2\left(1-\frac{T}{E_\nu}\right)^2\end{aligned}$$

$$-\left\{(g_L^\nu g_V^e)^2-(g_L^\nu g_A^e)^2\right\}\frac{m_e T}{E_\nu^2}\Bigg]\ . \quad (6)$$

The upper and lower signs correspond to the neutrino and anti-neutrino cases, respectively. In this equation, E_ν is the incident ν_μ energy and T is the electron recoil kinetic energy.

More often in the literature, the cross section is defined in terms of the parameters $(g_V^{\nu e}, g_A^{\nu e})$, which are defined as

$$\begin{aligned} g_V^{\nu e} &\equiv (2g_L^\nu g_V^e) = \rho\left(-\frac{1}{2}+2\sin^2\theta_W\right)\ , \\ g_A^{\nu e} &\equiv (2g_L^\nu g_A^e) = \rho\left(-\frac{1}{2}\right)\ , \end{aligned} \quad (7)$$

In terms of these parameters, we can write:

$$\begin{aligned} \frac{d\sigma}{dT} &= \frac{G_F^2 m_e}{2\pi}\Bigg[(g_V^{\nu e}\pm g_A^{\nu e})^2 \\ &\quad +(g_V^{\nu e}\mp g_A^{\nu e})^2\left(1-\frac{T}{E_\nu}\right)^2 \\ &\quad -\left\{(g_V^{\nu e})^2-(g_A^{\nu e})^2\right\}\frac{m_e T}{E_\nu^2}\Bigg]\ . \end{aligned} \quad (8)$$

When $m_e \ll E_\nu$, as is the case in NuSOnG, the third term in these expressions can be neglected. If we introduce the variable $y = T/E_\nu$, then

$$\frac{d\sigma}{dy} = \frac{G_F^2 m_e E_\nu}{2\pi}\left[(g_V^{\nu e}\pm g_A^{\nu e})^2+(g_V^{\nu e}\mp g_A^{\nu e})^2(1-y)^2\right]\ . \quad (9)$$

Integrating, we obtain the total cross sections which are

$$\sigma = \frac{G_F^2 m_e E_\nu}{2\pi}\left[(g_V^{\nu e}\pm g_A^{\nu e})^2+\frac{1}{3}(g_V^{\nu e}\mp g_A^{\nu e})^2\right]\ . \quad (10)$$

Note that

$$\begin{aligned} (g_V^{\nu e}+g_A^{\nu e})^2 &= \rho^2\left(-1+2\sin^2\theta_W\right)^2 \\ &= \rho^2\left(1-4\sin^2\theta_W+4\sin^4\theta_W\right)\ , \\ (g_V^{\nu e}-g_A^{\nu e})^2 &= \rho^2\left(2\sin^2\theta_W\right)^2 \\ &= \rho^2\left(4\sin^4\theta_W\right)\ . \end{aligned} \quad (11)$$

Therefore,

$$\begin{aligned} \sigma(\nu_\mu\, e) &= \frac{G_F^2 m_e E_\nu}{2\pi}\,\rho^2\left[1-4\sin^2\theta_W+\frac{16}{3}\sin^4\theta_W\right]\ , \\ \sigma(\bar\nu_\mu\, e) &= \frac{G_F^2 m_e E_\nu}{2\pi}\,\frac{\rho^2}{3}\left[1-4\sin^2\theta_W+16\sin^4\theta_W\right]\ . \end{aligned} \quad (12)$$

The ratio of the integrated cross sections for neutrino to antineutrino electron ES is

$$R_{\nu/\bar\nu} = \frac{\sigma(\nu_\mu\, e)}{\sigma(\bar\nu_\mu e)} = 3\,\frac{1-4\sin^2\theta_W+\frac{16}{3}\sin^4\theta_W}{1-4\sin^2\theta_W+16\sin^4\theta_W}\ . \quad (13)$$

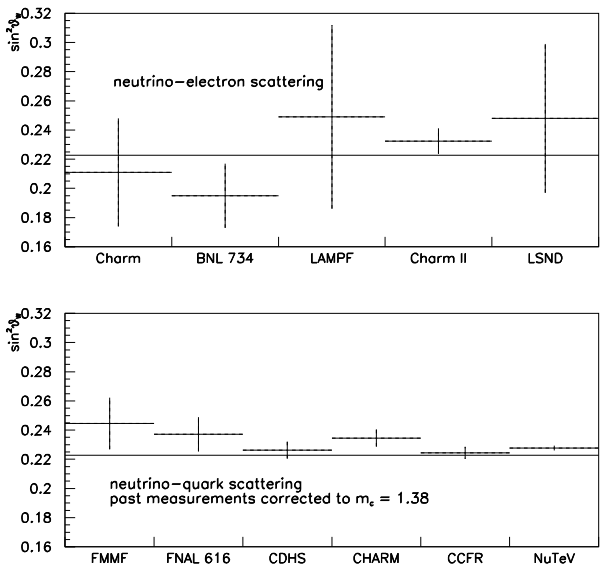

FIG. 4: Measurements of $\sin^2\theta_W$ from past experiments. Top: neutrino-electron elastic scattering experiments. Bottom: neutrino DIS experiments. All DIS results are adjusted to the same charm mass (relevant for experiments not using the PW method). The Standard Model value, indicated by the line, is 0.2227 [11].

Fig. 4(top) shows the results for $\sin^2\theta_W$ from many past experiments which have used this "$\nu/\bar\nu$ ES ratio."

In the ratio, $R_{\nu/\bar\nu}$, the dependence on ρ canceled. This directly extracts $\sin^2\theta_W$. The relationship between the error on the ratio and the error on $\sin^2\theta_W$, which for convenience we abbreviate as z, is:

$$\begin{aligned} \delta z &= \Big(\frac{32z-12}{16z^2-4z+1}+ \\ &\quad \frac{448z^2-144z-512z^3+12}{48z^2-8z-128z^3+256z^4+1}\Big)^{-1}\delta R_{\nu/\bar\nu} \\ &= -0.103\ \delta R_{\nu/\bar\nu}; \quad (14) \\ \delta z/z &= -0.575\ \delta R_{\nu/\bar\nu}/R_{\nu/\bar\nu}, \quad (15) \end{aligned}$$

for $z = 0.2227$ (or $R_{\nu/\bar\nu} = 1.242$). Roughly, the fractional error on $\sin^2\theta_W$ is 60% of the fractional error on $R_{\nu/\bar\nu}$.

B. A New Technique: Normalization Through IMD

An experiment such as NuSOnG can make independent measurements of the electroweak parameters for both ν_μ and $\bar\nu_\mu$-electron scattering. We can achieve this via ratios or by direct extraction of the cross section. In the case of ν_μ-electron scattering, we will use the ratio of

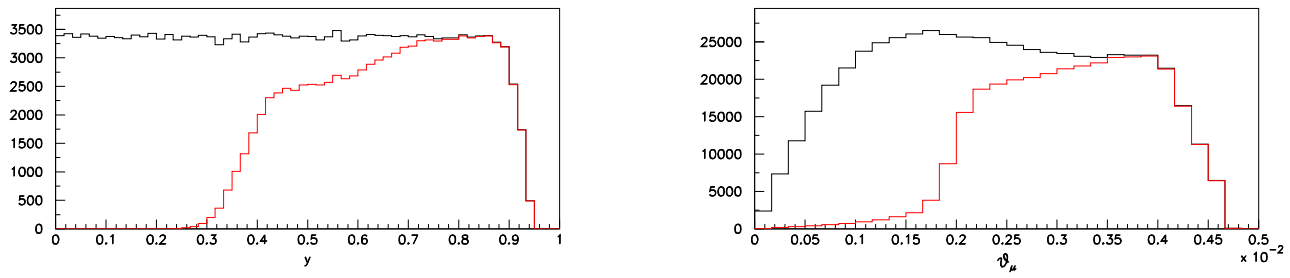

FIG. 5: Kinematic distributions for IMD events from incident neutrino energy between 100 and 200 GeV. Left: y distribution; right: θ_μ distribution. Black: distribution of events before cuts; Red: distribution after cuts for analysis method 1 (see Sec. III D).

the number of events in neutrino-electron elastic scattering to inverse muon decay:

$$\frac{N(\nu_\mu e^- \to \nu_\mu e^-)}{N(\nu_\mu e^- \to \mu^- \nu_e)} = \frac{\sigma^{\nu e}_{NC} \times \Phi^\nu}{\sigma^{IMD} \times \Phi^\nu}. \tag{16}$$

Because the cross section for IMD events is well determined by the Standard Model, this ratio should have low errors and will isolate the EW parameters from NC scattering. In the discussion below, we will assume that the systematic error on this ratio is 0.5%.

In the case of $\bar{\nu}_\mu$ data, the absolute normalization is more complex because there is no equivalent process to inverse muon decay (since there are no positrons in the detector). One can use the fact that, for low exchange energy (or "nu") in Deep Inelastic Scattering, the cross sections in neutrino and antineutrino scattering approach the same constant, A [12]. This is called the "low nu method" of flux extractions. For DIS events with low energy transfer and hence low hadronic energy ($5 \lesssim E_{had} \lesssim 10$ GeV), $N^{low\ E_{had}}_{\nu DIS} = \Phi^\nu A$ and $N^{low\ E_had}_{\bar{\nu} DIS} = \Phi^{\bar{\nu}} A$. The result is that the electroweak parameters can be extracted using the ratio

$$\frac{N^{low\ E_{had}}_{\nu DIS}}{N^{low\ E_{had}}_{\bar{\nu} DIS}} \times \frac{N(\bar{\nu}_\mu e^- \to \bar{\nu}_\mu e^-)}{N(\nu_\mu e^- \to \mu^- \nu_e)} = \frac{\Phi^\nu}{\Phi^{\bar{\nu}}} \times \frac{\sigma^{\bar{\nu} e}_{NC} \times \Phi^{\bar{\nu}}}{\sigma^{IMD} \times \Phi^\nu}. \tag{17}$$

The first ratio cancels the DIS cross section, leaving the energy-integrated ν to $\bar{\nu}$ flux ratio. The IMD events in the denominator of the second term cancel the integrated ν flux. The NC elastic events cancel the integrated $\bar{\nu}$ flux.

Because of the added layer of complexity, the antineutrino ES measurement would have a higher systematic error than the neutrino ES scattering measurement. The potentially higher error is one factor leading to the plan that NuSOnG concentrate on neutrino running for the ES studies.

As shown in Fig. 2, IMD events have a kinematic threshold at 10.9 GeV. These events also have other interesting kinematic properties. The minimum energy of the outgoing muon in the lab frame is given by

$$E^{min}_{\mu\ lab} = \frac{m_\mu^2 + m_e^2}{2m_e} = 10.9 \text{ GeV}. \tag{18}$$

In the detector described above, muons of this energy and higher will reach the toroid spectrometer without ranging-out in the glass. An interesting consequence is that, independent of E_ν, the energy transfer in the interaction has a maximum value of

$$y_{max} = 1 - \frac{10.9 \text{ GeV}}{E_\nu}. \tag{19}$$

Thus at low E_ν, the cutoff in y is less than unity, as shown in Fig. 5 (left). The direct consequence of this is a strong cutoff in angle of the outgoing muon, shown in Fig. 5 (right). In principle, one can reconstruct the full neutrino energy in these events:

$$E^{IMD}_\nu = \frac{1}{2} \frac{2m_e E_\mu - m_e^2 - m_\mu^2}{m_e - E_\mu + p_\mu \cos\theta_\mu} \tag{20}$$

This formula depends on θ_μ, which is small. The reconstructed E_ν is smeared by resolution effects as seen in Fig. 6. While the analysis can be done by summing over all energies, these distributions indicate that an energy binned analysis may be possible. This is more powerful because one can fit for the energy dependence of backgrounds. For the illustrative analyzes below, however, we do not employ this technique.

The error on $\sin^2\theta_W$ extracted from this ratio, $R_{ES/IMD}$, assuming a Standard Model value for ρ, is the same as the error on the ratio:

$$\frac{\delta(sin^2\theta_W)}{sin^2\theta_W} \approx \frac{\delta R_{ES/IMD}}{R_{ES/IMD}}. \tag{21}$$

Ref. [13] provides a useful summary of radiative corrections for the ES and IMD processes, which were originally calculated in Ref. [14]. The error from radiative

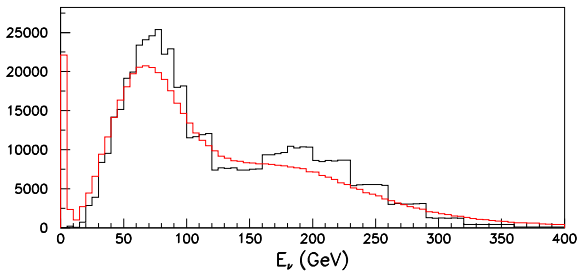

FIG. 6: Reconstructed neutrino energy (red) for IMD events before cuts compared to true neutrino energy (black).

corrections is expected to be below 0.1%. It is noted that to reduce the error below 0.1%, leading two-loop effects must be included. A new evaluation of the radiative corrections is underway [15].

C. IMD Normalization vs. $\bar{\nu}$ Normalization

NuSOnG can measure both the $\nu/\bar{\nu}$ ES ratio, as in the case of past experiments shown in Eq. (13), as well as the ES/IMD ratio. In the case of the former, to obtain the best measurement in a 5 year run, one would choose a 1:3 ratio of run time in ν versus $\bar{\nu}$ mode. In the latter case, one would maximize running in ν mode. The result of the two cases is a nearly equal error on $\sin^2\theta_W$, despite the fact that the error on the $\nu/\bar{\nu}$ ES is nearly twice that of the ES/IMD ratio. To understand this, compare Eq. (15) to Eq. (21). However, the ES/IMD ratio is substantially stronger for reasons of physics. Therefore, our conceptual design calls for running mainly with a ν beam. In this section we explore the issues for these two methods of measurement further. We also justify why the precision measurement requires high energies, only available from a Tevatron-based beam.

1. *Comparison of the Two Measurement Options*

From the point of view of physics, The ES/IMD ratio is more interesting than the $\nu/\bar{\nu}$ ES ratio. This is because ρ has canceled in the $\nu/\bar{\nu}$ ES ratio of Eq. (13), leaving the ratio insensitive to physics which manifests itself through changes in the NC coupling. Many of the unique physics goals of NuSOnG, discussed in Sec. IV, depend upon sensitivity to the NC coupling.

An equally important concern was one of systematics. The ν and $\bar{\nu}$ fluxes for a conventional neutrino beam are substantially different. For the case of NuSOnG, the fluxes are compared in Fig. 3. Predicting the differences in these fluxes from secondary production measurements and simulations leads to substantial systematic errors. For beams at high energies (> 30 GeV), such as NuSOnG, the "low nu" method [12] for determining the ratio of the neutrino to antineutrino fluxes from Deep Inelastic events, developed by CCFR and NuTeV and described in Sec. III B, can be employed. However, this leads to the criticism that one has introduced a new process into the purely-leptonic analysis.

Neither criticism is relevant to the ES/IMD ratio. The sensitivity to the new physics through the couplings does not cancel. Because both processes are in neutrino mode, the flux exactly cancels, as long as the neutrino energies are well above the IMD threshold (this will be illustrated in the analysis presented in Sec. III D). This ratio has the added advantage of needing only neutrino-mode running, which means that very high statistics can be obtained. This is clearly the more elegant solution.

It should be noted that nothing precludes continued running of NuSOnG beyond the 5-year plan presented here. This run-length was selected as "reasonable" for first results. If interesting physics is observed in this first phase, an extended run in antineutrino mode may be warranted, in which case *both* the ES/IMD and $\nu/\bar{\nu}$ ES ratios could be measured. The latter would then constrain $\sin^2\theta_W$ in a pure neutrino measurement and the former is then used to extract ρ.

To measure the ES/IMD ratio to high precision, there must be little low energy flux. This is because the IMD has a threshold of 10.9 GeV, and does not have substantial rate until ~ 30 GeV. The low-energy cut-off in the flux (see Fig. 3) coming from the energy-angle correlation of neutrinos from pion decay, is ideal.

2. *Why a Tevatron-based Beam is Best for Both Options*

The ES/IMD measurement is not an option for the planned beams from the Main Injector at Fermilab. For both presently planned Main Injector experiments at Fermilab [16] and for the proposed Project-X DUSEL beam [17], the neutrino flux is peaked at $\sim$5 GeV. The majority of the flux of these beams is below 5 GeV, and most of the flux is below the 10.9 GeV IMD threshold. Because of this, one simply cannot use the IMD events to normalize.

In principle, the $\nu/\bar{\nu}$ ES ratio could be used. However, in practice this will have large systematics. The ν and $\bar{\nu}$ fluxes for a horn beam are significantly different. First principles predictions of secondary mesons are not sufficient to reduce this error to the precision level. The energy range is well below the deep inelastic region where the "low nu" method can be applied to accurately extract a $\bar{\nu}/\nu$ flux ratio. Other processes, such as charged-current quasi-elastic scattering, could be considered for normalization, but the differences in nuclear effects in neutrino and antineutrino scattering for these events is not sufficiently well understood to yield a precision measurement.

Lastly, the ES rates for the present Main Injector beams are too low for a high statistics measurement.

This is because the cross section falls linearly with energy. Event samples on the order of 10k may be possible with extended running in the Project X DUSEL beam in the future. From the point of view of statistics, even though two orders of magnitude more protons on target are supplied in such a beam, the Tevatron provides a substantially higher rate of ES per year of running.

Compared to the Main Injector beam, a Tevatron-based beam does not face these issues. The choice of running in neutrino mode provides the highest precision measurement while optimizing the physics.

D. A 0.7% Measurement Goal for the ES to IMD Ratio

Achieving 0.7% precision on the ES/IMD measurement depends on reducing the backgrounds to an acceptable level without introducing significant systematics and while maintaining high signal statistics. Many of the systematic uncertainties will tend to cancel. The most important background for both the ν-e neutral current and IMD events comes from charged current quasi-elastic (CCQE) scatters ($\nu_e n \rightarrow pe$ and $\nu_\mu n \rightarrow p\mu$). These background CCQE processes have a much broader Q^2 as compared to the signal processes and, therefore, can be partially eliminated by kinematic cuts on the outgoing muon or electron. Initial cuts on the scattering angle and energy of the outgoing muon or electron can easily reduce the CCQE background by factors of 60 and 14 respectively while retaining over 50% of the ν-e neutral current and IMD signal. This leaves events with very forward scatters and outgoing scattered protons of low kinetic energy.

Because the NuSOnG design is at the conceptual stage and in order to be conservative, we have developed two different strategies for achieving a 0.7% error. This serves as a proof of principle that this level of error, or better, can be reached. The first method relies on detecting protons from the quasi-elastic scatter. The second method uses the beam kinematics to cut the low energy flux which reduces the CCQE background.

These methods were checked via two, independently written, parameterized Monte Carlos. The parameterized Monte Carlos made the assumptions given in Table II where both the assumed values and uncertainties are presented. These estimates of resolutions and systematic errors are based on previous experimental measurements or on fits to simulated data. One Monte Carlo used the Nuance event generator [19] to produce events, while the other was an independently written event generator. Both Monte Carlos include nuclear absorption and binding effects.

The first strategy uses the number of protons which exit the glass to constrain the total rate of the background. In $\sim$ 33% of the events, a proton will exit the glass, enter a chamber and traverse the gas. This samples protons of all energies and Q^2, since the interactions occur uniformly throughout the glass. After initial cuts, the protons are below 100 MeV, and therefore highly ionizing. If we define 1 MIP as the energy deposited by a single minimum ionizing particle, like a muon, then the protons consistently deposit greater than 5 MIPs in the chamber. Thus, one can identify CCQE events by requiring >4 MIPS in the first chamber. The amount of remaining CCQE background after this requirement can be measured if a fraction such as 10% of the detector is made from scintillating glass that can directly identify CCQE events from light associated with the outgoing proton. A wide range of scintillating glasses have been developed [20] for nuclear experiments. These glasses are not commonly used in high energy physics experiments because the scintillation time constant is typically on the order of 100 ns. In a neutrino experiment, which has inherently lower rates than most particle experiments, this is not an issue. CCQE events can be identified by the scintillation light from the proton assuming reasonable parameters for the glass and readout photomultiplier tubes: 450 photons/MeV, an attenuation length of 2 m, eight phototubes per glass sheet, quantum efficiency of the tubes of 20%. Using the identified CCQE events from the instrumented glass, the uncertainty in the residual background can be reduced to 2.0% for the IMD measurement. For the CCQE background to the ν_μ-e neutral current measurement, the uncertainty is assumed to be 3% for the Monte Carlo prediction. Combining all the systematic errors leads to a $\sim$0.7% accuracy on the ν-e measurement as shown in Tab. III.

In Tab. III, the cancellation of the flux errors should be noted. This occurred because we use the ES/IMD ratio, as discussed in the previous section.

The second strategy involves reducing the relative CCQE background to signal by using a harder flux for the analysis. This study used the same Monte Carlos, with the resolutions listed in Tab. II, as the first analysis. The total systematic and statistical error achieved was 0.6%. Below, we explain how a harder flux is obtained for the analysis. Then, we explain how this flux improves the signal-to-background in both the ES and IMD analyzes.

The strong correlation between energy and angle at the NuSOnG detector is used to isolate the harder flux. This is simplest to express in the non-bend view of the beamline, where it is given for pions by the well-known off-axis formula:

$$E_\nu = \frac{0.43 E_\pi}{1 + \gamma^2 \theta^2}, \tag{22}$$

where θ is the off-axis angle, $\gamma = E_\pi / m_\pi$, E_π is the energy of the pion and E_ν is the energy of the neutrino. For the NuTeV beam and detector lay-out, this angle-energy dependence resulted in the sharp cutoff of the flux for < 30 GeV shown in Fig. 3. Using the NuTeV G3 beam Monte Carlo [6], we have shown that by selecting vertices in the central region of the detector, one can adjust the energy where the flux sharply cuts off. Adjusting the aperture to retain flux above 50 GeV reduces the total

Quantity	Assumed Value	Uncertainty	Source of Estimate
Muon			
Energy Resolution	$\delta E/E = 10\%$	2.5%	NuTeV testbeam measurement
Energy Scale Error	$E_{rec} = 1.0 \times E_{true}$	0.5%	NuTeV testbeam measurement
Angular Resolution	$\delta\theta = 0.011/E^{0.96}$ rad	2.5%	Multiple scattering fit simulation
Electron			
Energy Resolution	$\delta E/E = 0.23/E^{0.5}$	1.0%	Same as CHARM II
Energy Scale Error	$E_{rec} = 1.0 \times E_{true}$	1.0%	Scaled from CHARM II with NuSOnG statistics
Angular Resolution	$\delta\theta = 0.008/E^{0.5}$ rad	2.5%	2 better than CHARM II due to sampling
Flux			
Normalization	1.0	3%	Current total cross section uncertainty
Shape Uncertainty	1.0	1%	Similar to NuTeV low-nu method
Backgrounds			
ν_μ CCQE	1.0	5%	Extrapolated from NuTeV
ν_e CCQE	1.0	3%	Extrapolated from CHARM II

TABLE II: Resolutions and systematic uncertainty estimates used in the parameterized Monte Carlo studies. The NuTeV estimates are based on Ref. [18] and the CHARM II estimates from Ref. [8]. Units for angles are radians and energies are in GeV.

	IMD Uncertainty	ES Uncertainty	Uncertainty on Ratio
Statistical Uncertainty	0.18%	0.46%	0.49%
Resolution Smearing			
$\delta(\mathrm{E}_\mu) = \pm 2.5\%$	0.00%	0.00%	0.00%
$\delta(\theta_\mu) = \pm 2.5\%$	0.04%	0.00%	0.04%
$\delta(\mathrm{E}_e) = \pm 1.5\%$	0.00%	0.01%	0.01%
$\delta(\theta_e) = \pm 2.5\%$	0.00%	0.09%	0.09%
Energy Scale			
$\delta(\mathrm{Escale}_\mu) = 0.5\%$	0.37%	0.00%	0.37%
$\delta(\mathrm{Escale}_e) = 1.5\%$	0.00%	0.19%	0.19%
Flux			
Normalization	3.00%	3.00%	0.00%
High energy flux up 1%	0.25%	0.25%	0.00%
Low energy flux up 1%	0.15%	0.13%	0.02%
IMD Background: statistical error	0.06%	0.00%	0.06%
2.0% systematic error	0.26%	0.00%	0.26%
ν_μe Background: statistical error	0.00%	0.12%	0.12%
3% systematic error	0.00%	0.19%	0.19%
		Total Syst. Uncertainty on Ratio	0.54%
		Total Stat. Uncertainty on Ratio	0.51%
		Total Uncertainty on Ratio	0.74%

TABLE III: Estimates of the IMD and ES uncertainties using a > 5 MIP cut on the first downstream chamber. The columns give the errors for each process and then for the ratio. Errors are included for statistical uncertainties and uncertainties associated with the knowledge of resolution smearing, energy scale, flux shape, and backgrounds. The flux shape uncertainties are significantly reduced in the ratio measurement.

event rate by 55%.

A harder flux allows for background reduction in both the ES and the IMD samples while maintaining the signal at high efficiency. In the case of ES events, the background is from ν_e CCQE. The energy distribution of the electron is substantially different in the two cases. In the case of ν_e CCQE events, the electron carries most of the energy of the incoming neutrino because the exchange energy in the interaction is small. Thus the CCQE events produced by the harder flux populate the visible energy range above 50 GeV. On the other hand, the outgoing electron in ES events tends to populate the low visible energy region due to the combination of a flat y distribution for the process convoluted with the incident neutrino energy spectrum. The result is that a cut on the visible energy less than 50 GeV reduces the error from the ν_e CCQE background to a negligible level. To understand the improvement in the IMD analysis, consider Fig. 2, which shows the threshold effects. The IMD signal is also rising with energy. In contrast, the ν_μ CCQE rate, which is the most significant background, is flat with energy for fluxes above 1 GeV. This signal-to-background is greatly

improved with a high energy flux. This allows looser cuts to be applied, which in turn reduces the systematics.

These two analyzes use substantially different strategies and can, in principle, be combined. Given these preliminary studies, we feel confident that as the detector moves from a conceptual to real design, we will be able to achieve a better than 0.7% error. However, for this paper we take the conservative approach of assuming 0.7%.

E. Neutrino Quark Scattering

Substantially higher precision has been obtained using neutrino-quark scattering, which compares neutral-current (NC) to charged-current (CC) scattering to extract $\sin^2\theta_W$. However, these experiments are subject to issues of modeling in the quark sector. Fig. 4(bottom) reviews the history of these measurements.

The lowest systematic errors come from implementing a "Paschos-Wolfenstein style" [5] analysis. This PW technique would be used by any future experiment, including NuSOnG. This requires high purity ν and $\bar{\nu}$ beams, for which the following ratios of DIS events could be formed:

$$R^{\nu} = \frac{\sigma^{\nu}_{NC}}{\sigma^{\nu}_{CC}} \quad (23)$$

$$R^{\bar{\nu}} = \frac{\sigma^{\bar{\nu}}_{NC}}{\sigma^{\bar{\nu}}_{CC}}. \quad (24)$$

Paschos and Wolfenstein [5] recast these as:

$$R^{-} = \frac{\sigma^{\nu}_{NC} - \sigma^{\bar{\nu}}_{NC}}{\sigma^{\nu}_{CC} - \sigma^{\bar{\nu}}_{CC}} = \frac{R^{\nu} - rR^{\bar{\nu}}}{1-r}, \quad (25)$$

where $r = \sigma^{\bar{\nu}}_{CC}/\sigma^{\nu}_{CC}$. In R^- many systematics cancel to first order, including the effects of the quark and antiquark seas for u, d, s, and c. Charm production only enters through $d_{valence}$ (which is Cabibbo suppressed) and at high x; thus the error from the charm mass is greatly reduced. The cross section ratios can be written in terms of the effective neutrino-quark coupling parameters g^2_L and g^2_R as

$$R^{\nu} = g^2_L + r g^2_R \quad (26)$$

$$R^{\bar{\nu}} = g^2_L + \frac{1}{r} g^2_R \quad (27)$$

$$R^{-} = g^2_L - g^2_R = \rho^2(\frac{1}{2} - \sin^2\theta_W), \quad (28)$$

in which

$$g^2_L = (2g^{\nu}_L g^u_L)^2 + (2g^{\nu}_L g^d_L)^2 = \rho^2(\frac{1}{2} - \sin^2\theta_W + \frac{5}{9}\sin^4\theta_W) \quad (29)$$

$$g^2_R = (2g^{\nu}_L g^u_R)^2 + (2g^{\nu}_L g^d_R)^2 = \rho^2(\frac{5}{9}\sin^4\theta_W). \quad (30)$$

In a variation on the PW idea, rather than directly form R^-, NuTeV fit simultaneously for R^{ν} and $R^{\bar{\nu}}$ to extract $\sin^2\theta_W$, obtaining the value $\sin^2\theta_W = 0.2277 \pm 0.00162$. Events were classified according to the length of hits in the scintillator planes of the NuTeV detector, with long events identified as CC interactions and short events as NC. An important background in the CC sample came from pion decay-in-flight, producing a muon in a NC shower. Significant backgrounds in the NC sample came from muons which ranged out or exited and from ν_e CC scatters which do not have a muon and thus are classified as "short."

In this paper, we present the sensitivity of NuSOnG to new physics if the NuTeV errors are reduced by a factor of ~ 2. This is a very conservative estimate, since most of the improvement comes from higher statistics. Only a 90% improvement in the systematics is required to reach this goal. Tab. IV argues why a 90% reduction in systematic error should be straightfroward to achieve. It is likely that the NuSOnG errors will be lower, but this requires detailed study.

In Table IV, we list the errors which NuTeV identified in their original analysis and indicate how NuSOnG will improve each error. Many of the largest experimental systematics of NuTeV are improved by introducing a fine-grained sampling calorimeter. The NuTeV detector had four inches of iron between unsegmented scintillator planes and eight inches between drift chamber planes. Better lateral segmentation and transverse detection will improve identification of scatters from intrinsic ν_es in the beam and separation of CC and NC events by improved three-dimensional shower shape analyzes. The NuTeV analyzes of the intrinsic ν_e content [21] and the CC/NC separation for the $\sin^2\theta_W$ analysis which relied strictly on event length. With this said, the power of classifying by event length is shown by the fact that the NuTeV intrinsic ν_e analysis was sensitive to a discrepancy in the predicted intrinsic ν_e rate which was recently resolved with a new measurement of the K_{e3} branching ratio that was published in 2003. Details of these issues are considered in the next section.

F. The NuTeV Anomaly

From Fig. 4, it is apparent that the NuTeV measurement is in agreement with past neutrino scattering results, although these have much larger errors; however, in disagreement with the global fits to the electroweak data which give a Standard Model value of $\sin^2\theta_W = 0.2227$ [24]. Expressed in terms of the couplings, NuTeV measures:

$$g^2_L = 0.30005 \pm 0.00137 \quad (31)$$

$$g^2_R = 0.03076 \pm 0.00110, \quad (32)$$

Source	NuTeV Error	Method of reduction in NuSOnG
Statistics	0.00135	Higher statistics
ν_e, $\bar{\nu}_e$ flux prediction	0.00039	Improves in-situ measurement of $\bar{\nu}_e$ CC scatters, thereby constraining prediction, due to better lateral segmentation and transverse detection. Also, improved beam design to further reduce $\bar{\nu}_e$ from K^0.
Interaction vertex position	0.00030	Better lateral segmentation.
Shower length model	0.00027	Better lateral segmentation and transverse detection will allow more sophisticated shower identification model.
Counter efficiency and noise	0.00023	Segmented scintillator strips of the type
		developed by MINOS [22] will improve this.
Energy Measurement	0.00018	Better lateral segmentation.
Charm production, strange sea	0.00047	In-situ measurement, See Sec. VI.
R_L	0.00032	In-situ measurement, see Sec. VI.
σ^ν/σ^ν	0.00022	Likely to be at a similar level.
Higher Twist	0.00014	Recent results reduce this error [23].
Radiative Corrections	0.00011	New analysis underway, see text below.
Charm Sea	0.00010	Measured in-situ using wrong-sign muon production in DIS.
Non-isoscalar target	0.00005	Glass is isoscalar

TABLE IV: Source and value of NuTeV errors on $\sin^2\theta_W$, and reason why the error will be reduced in the PW-style analysis of NuSOnG. This paper assumes NuSOnG will reduce the total NuTeV error by a factor of two. This is achieved largerly through the improved statistical precision and requires only a 90% reduction in the overal NuTeV systematic error. This table argues that a better than 90% reduction is likely, but further study, once the detector design is complete, is required.

which can be compared to the Standard Model values of $g_L^2 = 0.3042$ and $g_R^2 = 0.0301$, respectively.

NuTeV is one of a set of $Q^2 \ll m_Z^2$ experiments measuring $\sin^2\theta_W$. It was performed at $Q^2 = 1$ to 140 GeV^2, $\langle Q_\nu^2\rangle = 26$ GeV^2, $\langle Q_{\bar{\nu}}^2\rangle = 15$ GeV^2, which is also the expected range for NuSOnG. Two other precision low Q^2 measurements are from atomic parity violation [25] (APV), which samples $Q^2 \sim 0$; and SLAC E158, a Møller scattering experiment at average $Q^2 = 0.026$ GeV^2 [26]. Using the measurements at the Z-pole with $Q^2 = M_z^2$ to fix the value of $\sin^2\theta_W$, and evolving to low Q^2[27], the APV and SLAC E158 are in agreement with the Standard Model. However, the radiative corrections to neutrino interactions allow sensitivity to high-mass particles which are complementary to the APV and Møller-scattering corrections. Thus, these results may not be in conflict with NuTeV. The NuSOnG measurement will provide valuable additional information on this question.

Since the NuTeV result was published, more than 300 papers have been written which cite this result. Several "Standard-Model" explanations have been suggested. While some constraints on these ideas can come from outside experiments, it will be necessary for any future neutrino scattering experiment, such as NuSOnG, to be able to directly address these proposed solutions. Also various Beyond Standard Model explanations have been put forward; those which best explain the result require a follow-up experiment which probes the neutral weak couplings specifically with neutrinos, such as NuSOnG. Here, we consider the explanations which are "within the Standard Model" and address the Beyond Standard Model later.

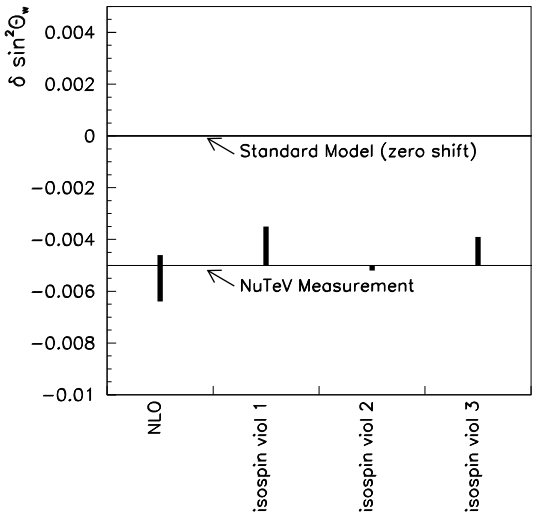

FIG. 7: Effect of various "Standard Model" explanations on the NuTeV anomaly. The y-axis is the deviation ($\delta\sin^2\theta_W = \sin^2\theta_W^{SM} - \sin^2\theta_W^{NuTeV}$). The solid line is the published NuTeV deviation. Thick black lines extending from the NuTeV deviation show the range of possible pulls from NLO QCD and various isospin violation models. Note that the isospin violation models are mutually exclusive and so should not be added in quadrature. They are, from left to right, the full bag model, the meson cloud model, and the isospin QED model.

Several systematic adjustments to the NuTeV result have been identified since the result was published but have not yet been incorporated into a new NuTeV analysis. As discussed here, the corrections due to the two new inputs, a new K_{e3} branching ratio and a new strange sea symmetry, are significant in size but are in opposite direction – away and toward the Standard Model. So a re-analysis can be expected to yield a central value for NuTeV which will not change significantly. However, the error is expected to become larger.

In 2003, a new result from BNL865 [28] yielded a K_{e3} branching ratio which was 2.3σ larger than past measurements and a value of $|V_{us}|^2$ which brought the CKM matrix measurements into agreement with unitarity in the first row [29]. The measurement was confirmed by CERN NA48/2 [30]. The resulting increased K_{e3} branching ratio [11] increases the absolute prediction of intrinsic ν_es in the NuTeV beam. This does not significantly change the error because the error on $Ke3$ was already included in the analysis. However, it introduces a correction moving the NuTeV result further away from the Standard Model, since it implies that in the original analysis, NuTeV under-subtracted the ν_e background in the NC sample. The shift in $\sin^2\theta_W$ can be estimated in a back of envelope calculation to be about $\sim$0.001 away from the Standard Model [31].

The final NuTeV measurement of the difference between the strange and anti-strange sea momentum distributions, was published in 2007 [32]. This "strange sea asymmetry" is defined as

$$xs^-(x) \equiv xs(x) - x\bar{s}(x), \tag{33}$$

Because of mass suppression for the production of charm in CC scatters from strange quarks, a difference in the momentum distributions will result in a difference in the CC cross sections for neutrinos and antineutrinos. Thus a correction to the denominator of Eq. (25) would be required. The most recent next-to-leading order analysis finds the asymmetry, integrated over x is $0.00195 \pm 0.00055 \pm 0.00138$ [32]. An integrated asymmetry of 0.007 is required to explain the published NuTeV result [32], and so one can estimate that this is a shift of about 0.0014 in $\sin^2\theta_W$ toward the Standard Model. In this case, the errors on the NuTeV result will become larger because this effect was not originally considered in the analysis. A very naive estimate of the size of the increase can be derived by scaling the error on the integrated strange sea, quoted above, and is about 0.001 toward the Standard Model. If this naive estimate of the systematic error is borne out, then this could raise the NuTeV error on $\sin^2\theta_W$ from 0.0016 to 0.0018.

In ref. [33], additional electromagnetic radiative corrections have been suggested as a source of the discrepancy. However, this paper only considered the effect of these corrections on R^ν and not $R^{\bar{\nu}}$ and for fixed beam energy of $E_\nu = 80$ GeV. The structure of the code from these authors has also made it difficult to modify for use in NuTeV. This has prompted a new set of calculations by other authors which are now under way [15]. There are, as yet, only estimates for the approximate size of newly identified effects, which are small.

The NuTeV analysis was not performed at a full NLO level in QCD; any new experiment, such as NuSOnG will need to undertake a full NLO analysis. This is possible given recently published calculations [34, 35], including those on target mass corrections [36]. On Fig. 7, we show an early estimate of the expected size and direction of the pull [37]. On this plot, the solid horizontal line indicates the deviation of NuTeV from the Standard Model. The thick vertical lines, which emanate from the NuTeV deviation, show the range of pulls estimated for various explanations. The range of pull for the NLO calculation is shown on the left.

The last possibility is that there is large isospin violation (or charge symmetry violation) in the nucleus. The NuTeV analysis assumed isospin symmetry, that is, $u(x)^p = d(x)^n$ and $d(x)^p = u(x)^n$. Isospin violation can come about from a variety of sources and is an interesting physics question in its own right. NuSOnG's direct constraints on isospin violation are discussed in Sec. VI D, which also considers the constraints from other experiments.

Various models for isospin violation have been studied and their pulls range from less than 1σ away from the Standard Model to $\sim 1\sigma$ toward the Standard Model [38]. We have chosen three examples [38] for illustration on Fig. 7: the full bag model, the meson cloud model, and the isospin QED model. These are mutually exclusive models, so only one of these can affect the NuTeV anomaly.

IV. THE TERASCALE PHYSICS REACH OF NUSONG

Even when new states are too heavy to be produced at resonance in collisions they can make their presence known indirectly, as virtual particles which affect SM processes through interference with SM contributions to amplitudes. The new heavy states induce small shifts in observables from SM predictions, and conversely precise measurements of these observables can constrain or detect new physics at mass scales well above the energies of the colliding particles. In this way the precision neutrino scattering measurements at NuSOnG will place TeV-scale indirect constraints on many classes of new physics, or perhaps detect new physics by measuring deviations from SM predictions. The effects of new high-scale physics may be reduced to a small number of effective operators along with corresponding parameters which may be fit to data. Although the particular set of operators used depends on broad assumptions about the new physics, the approach gives a parameterization of new physics which is largely model-independent.

Topic	Contribution of NuSOnG Measurement
Oblique Corrections	Four distinct and complementary probes of S and T. In the case of agreement with LEP/SLD: ∼25% improvement in electroweak precision.
Neutrino-lepton NSIs	Order of magnitude improvement in neutrino-electron effective couplings measurements. Energy scale sensitivity up to ~ 5 TeV at 95% CL.
Neutrino-quark NSIs	Factor of two improvement in neutrino-quark effective coupling measurements. Energy scale sensitivity up to ~ 7 TeV at 95% CL.
Mixing with Neutrissimos	30% improvement on the e-family coupling in a global fit. 75% improvement on the μ-family coupling in a global fit.
Right-handed Couplings	Complementary sensitivity to g_R/g_L compared to LEP. Order of magnitude improvement compared to past experiments.

TABLE V: Summary of NuSOnG's contribution to general Terascale physics studies.

For concreteness we will assume that NuSOnG will be able to measure the neutrino ES/IMD ratio to a precision of 0.7%, $\sigma(\bar{\nu}_\mu e)$ (normalized as per Sec. III B) to 1.3%, and that NuSOnG will be able to halve the errors on NuTeV's measurement of DIS effective couplings, to $\Delta g_L^2 = 0.0007$ and $\Delta g_R^2 = 0.0006$ (where g_L and g_R were defined in Eqs. (29) and (30)).

We first parameterize new physics using the oblique parameters ST, which is appropriate when the important effects of the new physics appear in vacuum polarizations of gauge bosons. We next assume new physics effects manifest as higher-dimensional operators made of SM fermion fields. We separately consider the possibility that the gauge couplings to neutrinos are modified. Realistic models usually introduce several new operators with relations among the coefficients; we consider several examples. A summary of the contributions of NuSOnG to the study of Terascale Physics is provided in Table V.

A. Oblique corrections

For models of new physics in which the dominant loop corrections are vacuum polarization corrections to the $SU(2)_L \times U(1)_Y$ gauge boson propagators ("oblique" corrections), the STU [39, 40] parameterization provides a convenient framework in which to describe the effects of new physics on precision electroweak data. Differences between the predictions of a new physics model and those of a reference Standard Model (with a specified Higgs boson and top quark mass) can be expressed as nonzero values of the oblique correction parameters S, T and U. T and U are sensitive to new physics that violates isospin, while S is sensitive to isospin-conserving physics. Predictions of a Standard Model with Higgs or top masses different from the reference Standard Model may also be subsumed into shifts in S and T (in many models U is much smaller than S and T and is largely unaffected by the Higgs mass, so it is often omitted in fits). Within a specific model of new physics the shift on the ST plot away from the SM will be calculable [41]. For example,

- A heavy Standard Model Higgs boson will make a positive contribution to S and a larger negative contribution to T.
- Within the space of Z' models, a shift in almost any direction in ST space is possible, with larger shifts for smaller Z' masses.
- Models with a fourth-generation of fermions will shift S positive, and will shift T positive if there are violations of isospin.

In constructing models incorporating several types of new physics the corresponding shifts to S and T combine; if contributions from different sectors are large, then they must conspire to cancel.

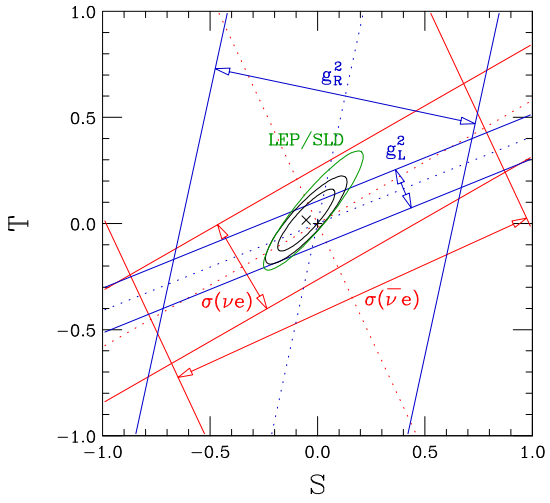

FIG. 8: The impact of NuSOnG on the limits of S and T. The reference SM is $m_t = 170.9$ GeV, and $m_H = 115$ GeV. 1σ bands due to NuSOnG observables are shown against the 90% contour from LEP/SLD. The central ellipses are the 68% and 90% confidence limit contours with NuSOnG included. See Eqs. (29) and (30) for the definitions of g_L and g_R.

The constraints on S and T from the full set of precision electroweak data strongly restrict the models of new

physics which are viable. The strongest constraints are from LEP/SLD, which give a current bound of

$$\begin{aligned} S &= -0.02 \pm 0.11 \,, \\ T &= +0.06 \pm 0.13 \,, \\ \mathrm{Corr}(S,T) &= 0.91. \end{aligned} \tag{34}$$

The ES and DIS measurements from NuSOnG provide four distinct and complementary probes of S and T, as shown in Fig. 8. If the target precision is achieved, and assuming the NuSOnG agree with SM predictions, NuSOnG will further reduce the errors on S and T from the LEP/SLD values to

$$\begin{aligned} S &= -0.05 \pm 0.09 \,, \\ T &= +0.02 \pm 0.10 \,, \\ \mathrm{Corr}(S,T) &= 0.87 \,. \end{aligned} \tag{35}$$

The $\sim 25\%$ reduction in the errors is primarily due to the improved measurement of g_L^2. We note that the error g_L^2 is likely to be further reduced (see Sec. III E), and so the this is conservative estimate of NuSOnG's contribution to the physics.

B. Non-standard interactions

NuSOnG will probe new physics that modifies neutrino-quark and neutrino-electron scattering. If the masses associated to the new degrees of freedom are much larger than the center of mass energy ($s = 2m_e E_{\rm beam} \lesssim 0.5$ GeV^2) then modifications to these processes are well-described by higher-dimensional effective operators. In the context of neutrino reactions, these operators are also referred to as non-standard interactions (NSI's). In a model-independent effective Lagrangian approach these effective operators are added to the SM effective Lagrangian with arbitrary coefficients. Expressions for experimental observables can be computed using the new effective Lagrangian, and the arbitrary coefficients can then be constrained by fitting to data. Typically, bounds on the magnitude of the coefficients are obtained using only one or a few of the available effective operators. This approach simplifies the analysis and gives an indication of the scale of constraints, although we must be mindful of relationships among different operators that will be imposed by specific assumptions regarding the underlying physics.

To assess the sensitivity of NuSOnG to "heavy" new physics in neutral current processes, we introduce the following effective Lagrangian for neutrino-fermion interactions [43, 47, 48]:

$$\begin{aligned} \mathcal{L}_{\rm NSI} &= -\sqrt{2} G_F \Big[\bar{\nu}_\alpha \gamma_\sigma P_L \nu_\beta \Big] \Big[\varepsilon^{fV}_{\alpha\beta} \, \bar{f} \gamma^\sigma f - \varepsilon^{fA}_{\alpha\beta} \, \bar{f} \gamma^\sigma \gamma_5 f \Big] \\ &= -2\sqrt{2} G_F \Big[\bar{\nu}_\alpha \gamma_\sigma P_L \nu_\beta \Big] \Big[\varepsilon^{fL}_{\alpha\beta} \, \bar{f} \gamma^\sigma P_L f \\ &\qquad + \varepsilon^{fR}_{\alpha\beta} \, \bar{f} \gamma^\sigma P_R f \Big] \,. \end{aligned} \tag{36}$$

where $\alpha, \beta = e, \mu, \tau$ and L, R represent left-chiral and right-chiral fermion fields. If $\alpha \neq \beta$, then the $\alpha \leftrightarrow \beta$ terms must be Hermitian conjugates of each other, *i.e.* $\varepsilon_{\beta\alpha} = \varepsilon^*_{\alpha\beta}$. NuSOnG is sensitive to the $\beta = \mu$ couplings. This effective Lagrangian is appropriate for parameterizing corrections to neutral current processes; an analysis of corrections to charged-current processes requires a different set of four-fermion operators.

Assuming $\varepsilon_{\alpha\beta} = 0$ for $\alpha \neq \beta$ we need consider only the terms $\varepsilon^{f*}_{\mu\mu}$ ($* = V, A, L, R$). If we rewrite Eq. (2) as

$$\begin{aligned} \mathcal{L} &= -\sqrt{2} G_F \Big[\bar{\nu} \gamma_\mu P_L \nu \Big] \Big[g_V^{\nu f} \, \bar{f} \gamma^\mu f - g_A^{\nu f} \, \bar{f} \gamma^\mu \gamma_5 f \Big] \\ &= -2\sqrt{2} G_F \Big[\bar{\nu} \gamma_\mu P_L \nu \Big] \Big[g_L^{\nu f} \, \bar{f} \gamma^\mu P_L f \\ &\qquad + g_R^{\nu f} \, \bar{f} \gamma^\mu P_R f \Big] \,, \end{aligned} \tag{37}$$

where

$$\begin{aligned} g_V^{\nu f} &= 2 g_L^\nu g_V^f = \rho \left(I_3^f - 2 Q^f \sin^2 \theta_W \right) \,, \\ g_A^{\nu f} &= 2 g_L^\nu g_A^f = \rho \left(I_3^f \right) \,, \\ g_L^{\nu f} &= 2 g_L^\nu g_L^f = \rho \left(I_3^f - Q^f \sin^2 \theta_W \right) \,, \\ g_R^{\nu f} &= 2 g_L^\nu g_R^f = \rho \left(-Q^f \sin^2 \theta_W \right) \,, \end{aligned} \tag{38}$$

then we see that adding Eq. (36) to the SM Lagrangian will simply shift the effective couplings:

$$\begin{aligned} g_V^{\nu f} &\longrightarrow \tilde{g}_V^{\nu f} = g_V^{\nu f} + \varepsilon^{fV}_{\mu\mu} \,, \\ g_A^{\nu f} &\longrightarrow \tilde{g}_A^{\nu f} = g_A^{\nu f} + \varepsilon^{fA}_{\mu\mu} \,, \\ g_L^{\nu f} &\longrightarrow \tilde{g}_L^{\nu f} = g_L^{\nu f} + \varepsilon^{fL}_{\mu\mu} \,, \\ g_R^{\nu f} &\longrightarrow \tilde{g}_R^{\nu f} = g_R^{\nu f} + \varepsilon^{fR}_{\mu\mu} . \end{aligned} \tag{39}$$

Consequently, errors on the $g_P^{\nu f}$'s translate directly into errors on the $\varepsilon^{fP}_{\mu\mu}$'s, $P = V, A$ or $P = L, R$.

1. Neutrino-lepton NSI

A useful review of present constraints on non-standard neutrino-electron interactions can be found in reference [44]. As this paper states, and as we show below, an improved measurement of neutrino-elecron scattering is needed.

The world average value for neutrino-electron effective couplings, dominated by CHARM II, is

$$\begin{aligned} g_V^{\nu e} &= -0.040 \pm 0.015 \,, \\ g_A^{\nu e} &= -0.507 \pm 0.014 \,, \\ \mathrm{Corr}(g_V^{\nu e}, g_A^{\nu e}) &= -0.05 \,. \end{aligned} \tag{40}$$

The current 1σ bounds from CHARM II, Eq. (40) translates to $|\varepsilon^{eP}_{\mu\mu}| < 0.01$, ($P = L, R$) with a correlation of 0.07 [43]. At the current precision goals, NuSOnG's $\nu_\mu e$ and $\overline{\nu}_\mu e$ will significantly reduce the uncertainties on these NSI's, to

$$\begin{aligned} |\varepsilon^{eV}_{\mu\mu}| &< 0.0036 \,, \\ |\varepsilon^{eA}_{\mu\mu}| &< 0.0019 \,, \end{aligned}$$

$$\mathrm{Corr}(\varepsilon^{eV}_{\mu\mu}, \varepsilon^{eA}_{\mu\mu}) \;=\; -0.57\,, \tag{41}$$

or in terms of the chiral couplings,

$$\begin{aligned} |\varepsilon^{eL}_{\mu\mu}| \;&<\; 0.0015\,, \\ |\varepsilon^{eR}_{\mu\mu}| \;&<\; 0.0025\,, \\ \mathrm{Corr}(\varepsilon^{eL}_{\mu\mu}, \varepsilon^{eR}_{\mu\mu}) \;&=\; 0.64.\,. \end{aligned} \tag{42}$$

Even in the absence of a $\sigma(\bar{\nu}_\mu e)$ measurement $\varepsilon^{eL}_{\mu\mu}$ and $\varepsilon^{eR}_{\mu\mu}$ can be constrained from the $\nu_\mu e$ scattering data alone through a fit to the recoil electron energy spectrum (see Eq. (9)).

We first consider the constraint on $\varepsilon^{eL}_{\mu\mu}$ and $\varepsilon^{eR}_{\mu\mu}$ from the total cross section $\sigma(\nu_\mu e)$. It is convenient to recast the effective interaction slightly, as

$$\begin{aligned} \mathcal{L}^{e}_{\mathrm{NSI}} \;&=\; -2\sqrt{2}G_F\Big[\,\bar{\nu}_\alpha\gamma_\sigma P_L\nu_\mu\,\Big]\Big[\,\varepsilon^{eL}_{\alpha\mu}\,\bar{e}\gamma^\sigma P_L e + \varepsilon^{eR}_{\alpha\mu}\,\bar{e}\gamma^\sigma P_R e\,\Big] \\ &=\; +\frac{\sqrt{2}}{\Lambda^2}\Big[\,\bar{\nu}_\alpha\gamma_\sigma P_L\nu_\mu\,\Big]\Big[\,\cos\theta\,\bar{e}\gamma^\sigma P_L e + \sin\theta\,\bar{e}\gamma^\sigma P_R e\,\Big]\,. \end{aligned} \tag{43}$$

The new physics is parameterized by two coefficients Λ and θ. Λ represents the broadly-defined new physics scale while $\theta \in [0, 2\pi]$ defines the relative coupling of left-chiral and right-chiral electrons to the new physics. As an example, a scenario with a purely "left-handed" Z' that couples to leptons with coupling g' would be described by $\Lambda \propto M_{Z'}/g'$ and $\theta = 0$ or $\theta = \pi$, depending on the relative sign between g' and the electroweak couplings. Λ and θ are related to to the NSI parameters in Eq. (36) by

$$\varepsilon^{eL}_{\alpha\mu} = -\frac{\cos\theta}{2G_F\Lambda^2}\,, \quad \varepsilon^{eR}_{\alpha\mu} = -\frac{\sin\theta}{2G_F\Lambda^2}. \tag{44}$$

Note that we have generalized from our assumption of the previous section and not taken $\alpha = \mu$ necessarily. At NuSOnG, new physics modifies (pseudo)elastic neutrino–electron scattering. Here we use the word "pseudo" to refer to the fact that we cannot identify the flavor of the final-state neutrino, which could be different from the incoming neutrino flavor in the case of flavor changing neutral currents.

The shift in the total cross section is

$$\begin{aligned} \frac{\delta\sigma(\nu_\mu e)}{\sigma(\nu_\mu e)} \;&=\; \frac{\left\{\,2\,g^{\nu e}_L\,\varepsilon^{eL}_{\mu\mu} + (\varepsilon^{eL}_{\mu\mu})^2\right\} + \frac{1}{3}\left\{\,2\,g^{\nu e}_R\,\varepsilon^{eR}_{\mu\mu} + (\varepsilon^{eR}_{\mu\mu})^2\right\}}{(g^{\nu e}_L)^2 + \frac{1}{3}(g^{\nu e}_R)^2} \\ &\approx\; -\left(\frac{516\,\mathrm{GeV}}{\Lambda}\right)^2\cos(\theta-\phi) \\ &\quad +0.096\left(\frac{516\,\mathrm{GeV}}{\Lambda}\right)^4(1+2\cos^2\theta)\,. \end{aligned} \tag{45}$$

where

$$\tan\phi \;=\; \frac{g^{\nu e}_R}{3g^{\nu e}_L} \;\approx\; -0.28\,. \tag{46}$$

When $\mathcal{O}(\varepsilon^2)$ terms are negligible, a 0.7% measurement of $\sigma(\nu_\mu e)$ translates into a 95% confidence level bound of

$$\Lambda \;>\; (4.4\,\mathrm{TeV}) \times \sqrt{|\cos(\theta-\phi)|} \tag{47}$$

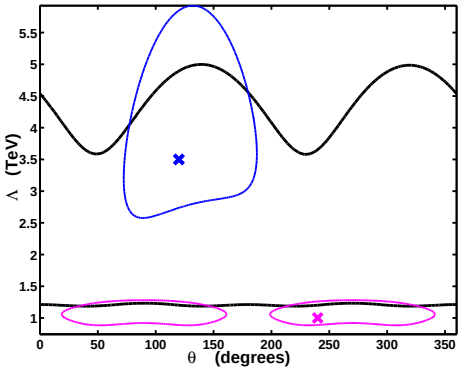

FIG. 9: (DARK LINES) 95% confidence level sensitivity of NuSOnG to new heavy physics described by Eq. (43) when $\nu_\alpha = \nu_\mu$ (higher curve) and $\nu_\alpha \neq \nu_\mu$ (lower curve). (CLOSED CONTOURS) NuSOnG measurement of Λ and θ, at the 95% level, assuming $\nu_\alpha = \nu_\mu$, $\Lambda = 3.5$ TeV and $\theta = 2\pi/3$ (higher, solid contour) and $\nu_\alpha \neq \nu_\mu$, $\Lambda = 1$ TeV and $\theta = 4\pi/3$ (lower, dashed contour). Note that in the pseudoelastic scattering case ($\nu_\alpha \neq \nu_\mu$) θ and $\pi + \theta$ are physically indistinguishable.

from elastic scattering.

The measurement of the electron recoil energy will allow us to do better. Fig. 9(dark line) depicts the 95% confidence level sensitivity of NuSOnG to the physics described by Eq. (43) when $\nu_\alpha = \nu_\mu$, obtained after fitting the recoil electron kinetic energy distribution. Fig. 9(closed contour) represents how well NuSOnG should be able to measure Λ and θ, at the 95% level. Weaker bounds from pseudoelastic scattering are also shown. We have not included "data" from $\bar{\nu}_\mu$–electron scattering. While there will be fewer of these events, they should qualitatively improve our ability to pin down the new physics parameters given the distinct dependency on $g^{\nu e}_V$ and $g^{\nu e}_A$ (see Sec. III A).

Eq. (43) does not include all effective dimension-six

operators that contribute to neutrino–electron (pseudo) elastic scattering. All neglected terms will either not contribute at NuSOnG, or were assumed to be suppressed with respect to Eq. (43). In turn, terms proportional to a right-handed neutrino current $\bar{\nu}_R\gamma_\sigma\nu_R$ lead to negligibly small effects since neutrino masses are negligibly small and we are dealing with neutrino beams produced by pion and muon decay (*i.e.*, for all practical purposes, we have a purely left-handed muon neutrino beam and a purely right-handed muon antineutrino beam). Chirality violating effective operators (e.g. $(\bar{\nu}_R\nu_L)(\bar{e}_L e_R)$), on the other hand, are expected to be suppressed with respect to Eq. (43) by terms proportional to neutrino masses and the electron mass (measured in units of Λ). The reason is that, in the limit of massless neutrinos or a massless electron, chiral symmetry is restored while such operators explicitly violate it. For the same reason, dimension-five magnetic moment-type operators ($\bar{\nu}\sigma_{\rho\sigma}\nu F^{\rho\sigma}$) have also been neglected.

We note also that Eq. (43) violates $SU(2)_L$ unless one also includes similar terms where $\nu_L \leftrightarrow \ell_L$ ($\ell = e, \mu, \tau$). In this case, certain flavor combinations would be severely constrained by electron–electron scattering and rare muon and tau decays. One way around such constraints is to postulate that the operators in Eq. (43) are dimension-eight operators proportional to $\bar{L}H^*\gamma_\sigma LH$, where L is the left-chiral lepton doublet and H is the Higgs scalar doublet. In this case, $1/\Lambda^2$ should be replaced by v^2/Λ^4, where $v = 246$ GeV is the scale of electroweak symmetry breaking.

Finally, another concern is whether modifications to the charged current neutrino–electron (pseudo)quasi-elastic scattering ((pseudo)IMD, $\nu_\mu e \to \nu_\alpha \mu$) can render the translation of NuSOnG data into constraints or measurements of θ and Λ less straightforward. This turns out not to be the case, since new physics contributions to $\nu_\mu e \to \nu_\alpha \mu$ are already very well constrained by precision studies of muon decay. Hence, given the provisos of the two previous paragraph, Eq. (43) is expected to capture all "heavy" new physics effects in (pseudo)elastic neutrino electron scattering.

2. *Neutrino-quark NSI*

We next consider the $f = u, d$ case. The change in the parameters g_L^2 and g_R^2 (see Eqs. (29,30)) due to the NSI's is

$$\begin{aligned} \Delta g_L^2 &= 2g_L^{\nu u}\varepsilon_{\mu\mu}^{uL} + 2g_L^{\nu d}\varepsilon_{\mu\mu}^{dL} \\ &\approx +0.69\,\varepsilon_{\mu\mu}^{uL} - 0.85\,\varepsilon_{\mu\mu}^{dL}\,, \\ \Delta g_R^2 &= 2g_R^{\nu u}\varepsilon_{\mu\mu}^{uR} + 2g_R^{\nu d}\varepsilon_{\mu\mu}^{dR} \\ &\approx -0.31\,\varepsilon_{\mu\mu}^{uR} + 0.15\,\varepsilon_{\mu\mu}^{dR}\,. \end{aligned} \tag{48}$$

so only these linear combinations are constrained. The bounds from NuTeV (rescaled to 1σ bounds from ref. [43]) are:

$$\begin{aligned} \varepsilon_{\mu\mu}^{uL} &= -0.0053 \pm 0.0020\,, \\ \varepsilon_{\mu\mu}^{dL} &= +0.0043 \pm 0.0016\,, \\ |\varepsilon_{\mu\mu}^{uR}| &< 0.0035\,, \\ |\varepsilon_{\mu\mu}^{dR}| &< 0.0073\,. \end{aligned} \tag{49}$$

These bounds are obtained by setting only one of the parameters be non-zero at a time. If NuSOnG reduces the errors on the NuTeV measurement of g_L^2 and g_R^2 by a factor of 2, the 1σ bounds on the NSI parameters are similarly reduced:

$$\begin{aligned} |\varepsilon_{\mu\mu}^{uL}| &< 0.001\,, \\ |\varepsilon_{\mu\mu}^{dL}| &< 0.0008\,, \\ |\varepsilon_{\mu\mu}^{uR}| &< 0.002\,, \\ |\varepsilon_{\mu\mu}^{dR}| &< 0.004\,. \end{aligned} \tag{50}$$

In terms of a new physics scale defined as $\Lambda = 1/\sqrt{2\,G_F\varepsilon}$, these constraints range from $\Lambda > 3\,\text{TeV}$ to $\Lambda > 7\,\text{TeV}$.

We note that neutrino-quark scattering will also be sensitive to NSIs which correct CC interactions. These interactions are not included in Eq. (36). If they are important, as is the case in some of the scenarios we treat later, a new analysis is necessary and the bounds above cannot be used. This is to be contrasted to the neutrino–lepton case, discussed in the previous subsection.

C. Neutrissimos, Neutrino Mixing and Gauge Couplings

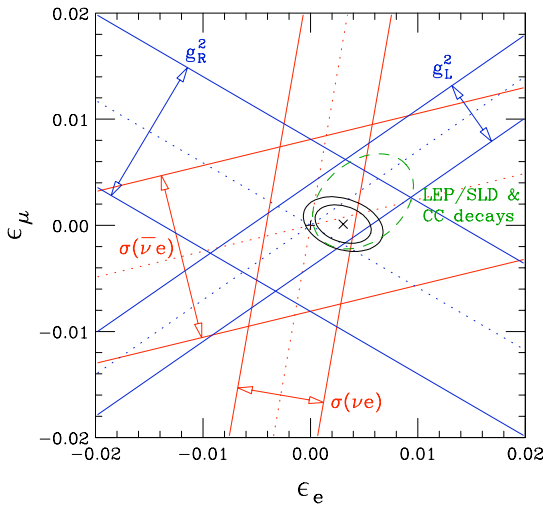

FIG. 10: Potential constraint on ϵ_e and ϵ_μ from NuSOnG (see Eq. (55)). This is a two-dimensional projection of a 4 parameter fit with S, T, ϵ_e and ϵ_μ. The green ellipse is the 90% CL contour of a fit to all the charge current particle decay data + LEP/SLD.

In those classes of models which include moderately heavy electroweak gauge singlet ("neutrissimo") states,

with masses above 45 GeV, the mixing of the $SU(2)_L$-active neutrinos and the sterile states may lead to a suppression of the neutrino-gauge couplings. The resulting pattern of modified interactions is distinct from those of the previous section since they will also induce correlated shifts to the charged-current coupling. For example, Ref. [45] presents models with one sterile state per active neutrino flavor and intergenerational mixing among neutrinos. In these models the flavor eigenstates are linear combinations of mass eigenstates, and those mass eigenstates too heavy to be produced in final states result in an effective suppression of the neutrino-gauge boson coupling. This suppression may be flavor-dependent depending on the structure of the neutrino mixing matrix. If the mass matrix contains Majorana terms, such models permit both lepton flavor violation and lepton universality violation.

Neutrinos couple to the W and the Z through interactions described by:

$$\begin{aligned}\mathcal{L} &= \frac{g}{\sqrt{2}} W_\mu^- \, \bar{\ell}_L \gamma^\mu \nu_{\ell L} + \frac{g}{\sqrt{2}} W_\mu^+ \, \bar{\nu}_{\ell L} \gamma^\mu \ell_L \\ &\quad + \frac{e}{2sc} Z_\mu \, \bar{\nu}_{\ell L} \gamma^\mu \nu_{\ell L} \, , \end{aligned} \tag{51}$$

where $\ell = e, \mu, \tau$. If the neutrinos mix with gauge singlet states so that the $SU(2)_L$ interaction eigenstate is a superposition of mass eigenstates $\nu_{\ell,\text{light}}$ and $\nu_{\ell,\text{heavy}}$

$$\nu_{\ell L} = \nu_{\ell,\text{light}} \cos\theta_\ell + \nu_{\ell,\text{heavy}} \sin\theta_\ell \, , \tag{52}$$

then the interaction of the light states is given by

$$\begin{aligned}\mathcal{L} &= \\ &\left(\frac{g}{\sqrt{2}} W_\mu^- \, \bar{\ell}_L \gamma^\mu \nu_{\ell,\text{light}} + \frac{g}{\sqrt{2}} W_\mu^+ \, \bar{\nu}_{\ell,\text{light}} \gamma^\mu \ell_L \right) \cos\theta_\ell \\ &+ \left(\frac{e}{2sc} Z_\mu \, \bar{\nu}_{\ell,\text{light}} \gamma^\mu \nu_{\ell,\text{light}} \right) \cos^2\theta_\ell \, . \end{aligned} \tag{53}$$

Defining

$$\epsilon_\ell \equiv 1 - \cos^2\theta_\ell \, . \tag{54}$$

the shift in the Lagrangian due to this mixing is

$$\begin{aligned}\delta\mathcal{L} &= -\left(\frac{g}{\sqrt{2}} W_\mu^- \, \bar{\ell}_L \gamma^\mu \nu_\ell + \frac{g}{\sqrt{2}} W_\mu^+ \, \bar{\nu}_\ell \gamma^\mu \ell_L \right) \frac{\epsilon_\ell}{2} \\ &- \left(\frac{e}{2sc} Z_\mu \, \bar{\nu}_\ell \gamma^\mu \nu_\ell \right) \epsilon_\ell \, , \end{aligned} \tag{55}$$

where we have dropped the subscript "light" from the neutrino fields.

Lepton universality data from W decays and from charged current π, τ and K decays [46] constraint differences $\epsilon_{\ell_i} - \epsilon_{\ell_j}$. LEP/SLD and other precision electroweak data will imposed additional constraints on ϵ_ℓ in combination with the oblique parameters, as will NuSOnG. A fit to all the charge current decay data and LEP/SLD with S, T, ϵ_e and ϵ_μ yields

$$\begin{aligned} S &= -0.05 \pm 0.11 \, , \\ T &= -0.44 \pm 0.28 \, , \\ \epsilon_e &= 0.0049 \pm 0.0022 \, , \\ \epsilon_\mu &= 0.0023 \pm 0.0021 \, . \end{aligned} \tag{56}$$

If we now included hypothetical data from NuSOnG, assuming NuSOnG achieves its precision goals and measures central values consistent with the Standard Model, we see the constraints on ϵ_μ and ϵ_e are substantially improved. In this case, the fit yields

$$\begin{aligned} S &= 0.00 \pm 0.10 \, , \\ T &= -0.11 \pm 0.12 \, , \\ \epsilon_e &= 0.0030 \pm 0.0017 \, , \\ \epsilon_\mu &= 0.0001 \pm 0.0012. \, , \end{aligned} \tag{57}$$

Fig. 10 shows the two dimensional cross section in the ϵ_e-ϵ_μ plane of the four dimensional fit. The likelihood coutours are 2D projections. Though not obvious from the figure, it is NuSOnG's improved measurement of g_L^2 which contributes the most to strengthening the bounds on the ϵ_ℓ.

In models of this class lepton flavor violating decays such as $\mu \to e\gamma$ impose additional constraints on products $\epsilon_{\ell_i}\epsilon_{\ell_j}$. For example, the strong constraint from $\mu \to e\gamma$ implies $\epsilon_e\epsilon_\mu \approx 0$. This type of model has been proposed as a solution to the NuTeV anomaly. If we take take only one of ϵ_e or ϵ_μ to be nonzero (to respect the constraint from $\mu \to e\gamma$), the NuTeV value of g_L^2 is accommodated in the fit by best-fit values of ϵ that are large and positive and best-fit values of T are large and negative (consistent with a heavy Higgs).

D. Right-handed coupling of the neutrino to the Z

In the Standard Model, neutrino couplings to the W- and Z-bosons are purely left-handed. The fact that the neutrino coupling to the W-boson and an electron is purely left-handed is, experimentally, a well-established fact (evidence includes precision measurements of pion and muon decay, nuclear processes, etc.). By contrast, the nature of the neutrino coupling to the Z boson is, experimentally, far from being precisely established [49]. The possibility of a right-handed neutrino–Z-boson coupling is not included in the previous discussions, and is pursued separately in this subsection.

The best measurement of the neutrino coupling to the Z-boson is provided by indirect measurements of the invisible Z-boson width at LEP. In units where the Standard Model neutrino–Z-boson couplings are $g_L^\nu = 0.5$, $g_R^\nu \equiv 0$, the LEP measurement [50] translates into $(g_L^\nu)^2 + (g_R^\nu)^2 = 0.2487 \pm 0.0010$. Note that this result places no meaningful bound on g_R^ν.

Precise, model-independent information on g_L^ν can be obtained by combining $\nu_\mu + e$ scattering data from CHARM II and LEP and SLD data. Assuming model-independent couplings of the fermions to the Z-boson, $\nu_\mu + e$ scattering measures $g_L^\nu = \sqrt{\rho}/2$, while LEP and SLD measure the left and right-handed couplings of the

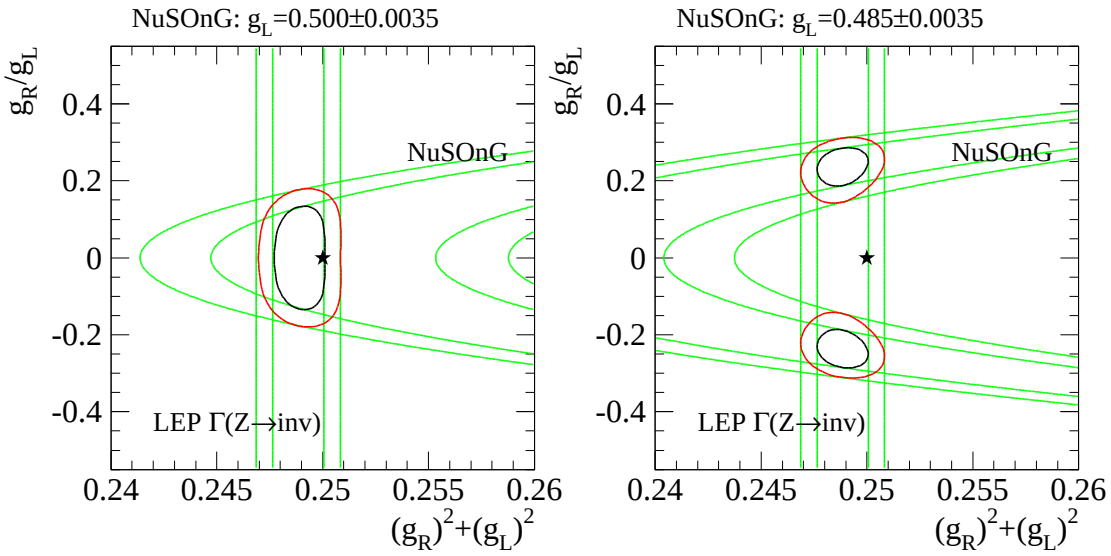

FIG. 11: Precision with which the right-handed neutrino–Z-boson coupling can be determined by combining NuSOnG measurements of g_L^ν with the indirect determination of the invisible Z-boson width at LEP if (left) the $\nu+e$ scattering measurement is consistent with the Standard Model prediction $g_L^\nu = 0.5$ and (right) the $\nu + e$ scattering measurement is significantly lower, $g_L^\nu = 0.485$, but still in agreement with the CHARM II measurement(at the one sigma level). Contours (black, red) are one and two sigma, respectively. The star indicates the Standard Model expectation.

electron to the Z. The CHARM II result translates into $|g_L^\nu| = 0.502 \pm 0.017$ [49], assuming that the charged-current weak interactions produce only left-handed neutrinos. In spite of the good precision of the CHARM II result (around 3.5%), a combination of all available data allows $|g_R^\nu/g_L^\nu| \sim 0.4$ at the two σ confidence level [49].

Significant improvement in our understanding of g_R^ν can only be obtained with more precise measurements of $\nu+e$ scattering, or with the advent of a new high intensity e^+e^- collider, such as the ILC. By combining ILC running at the Z-boson pole mass and at $\sqrt{s} = 170$ GeV, $|g_R^\nu/g_L^\nu| \lesssim 0.3$ could be constrained at the two σ level after analyzing $e^+e^- \to \gamma$+missing energy events [49].

Assuming that g_L^ν can be measured with 0.7% uncertainty, Fig. 11 depicts an estimate of how precisely g_R^ν could be constrained once NuSOnG "data" is combined with LEP data. Fig. 11(left) considers the hypothesis that the Standard Model expectations are correct. In this case, NuSOnG data would reveal that g_R/g_L is less than 0.2 at the two sigma level. On the other hand, if $g_R/g_L = 0.25$ – in good agreement with the current CHARM II and LEP data – NuSOnG data should reveal that $g_R \neq 0$ at more than the two sigma level, as depicted in Fig. 11(right).

The capability of performing this measurement in other experiments has been examined. The NuSOnG measurement compares favorably, and complements, the ILC capabilities estimated in [49]. Ref [51] studied measurements using other neutrino beams, including reactor fluxes and beta beams. NuSOnG's reach is equivalent to or exceeds the most optimistic estimates for these various neutrino sources.

V. SPECIFIC THEORETICAL MODELS AND EXPERIMENTAL SCENARIOS

If NuSOnG's measurements agree with the SM within errors, we will place stringent constraints on new physics models; if they disagree, it will be a signal for new physics. In the latter case the availability of both DIS and ES channels will improve our ability to discriminate among new physics candidates. NuSOnG will also provide an important complement to the LHC. The LHC will provide detailed information about the spectrum of new states directly produced. However, measurements of the widths of these new states will provide only limited information about their couplings. NuSOnG will probe in multiple ways the couplings of these new states to neutrinos and to other SM particles.

In this section we provide several case studies of NuSOnG sensitivity to specific models of new physics. These include several typical Z'models, leptoquark models, models of R-parity violating supersymmetry, and models with extended Higgs sectors. We examine how these will affect $\nu_\mu e$ ES and $\nu_\mu N$ DIS at tree-level. Our list is far from exhaustive but serves to illustrate the possibilities. We summarize our contributions in Table V.

The opposite way to approach this problem is to ask: in the face of evidence for new Terascale Physics, how can we differentiate between specific models? NuSOnG has the potential to *discover* new physics through indirect probes, in the event that one or more of its measurements definitively contradicts SM predictions. We

Model	Contribution of NuSOnG Measurement
Typical Z' Choices: $(B-xL)$,$(q-xu)$,$(d+xu)$	At the level of, and complementary to, LEP II bounds.
Extended Higgs Sector	At the level of, and complementary to τ decay bounds.
R-parity Violating SUSY	Sensitivity to masses ~ 2 TeV at 95% CL. Improves bounds on slepton couplings by $\sim 30\%$ and on some squark couplings by factors of 3-5.
Intergenerational Leptoquarks with non-degenerate masses	Accesses unique combinations of couplings. Also accesses coupling combinations explored by π decay bounds, at a similar level.

TABLE VI: Summary of NuSOnG's contribution in the case of specific models

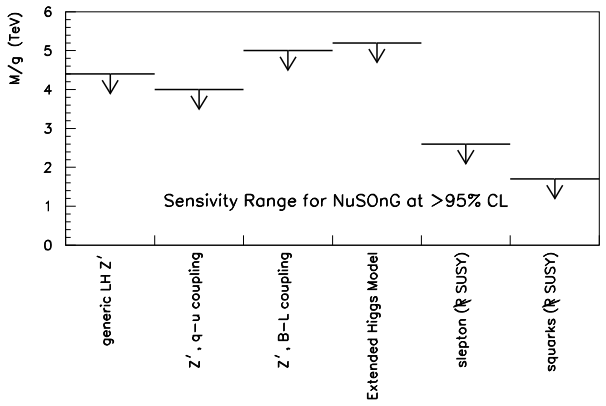

FIG. 12: Some examples of NuSOnG's 2σ sensitivity to new high-mass particles commonly considered in the literature. For explanation of these ranges, and further examples, see text.

discuss several possible patterns of deviation of model-independent parameters from SM predictions and some interpretations in terms of particular models. This is presented in the context of various expectations for LHC to illustrate how NuSOnG enhances the overall physics program. Since the NuTeV reanalysis is ongoing, and since the ES constraints from CHARM-II are weak, it is prudent that we commit to no strong assumptions about the central value of the NuSOnG measurements but instead consider all reasonable outcomes.

A. Sensitivity in the Case of Specific Theoretical Models

We next consider the constraints imposed by the proposed NuSOnG measurements on explicit models of BSM physics. An explicit model provides relations among effective operators which give stronger and sometimes better-motivated constraints on new physics than is obtained from bounds obtained by considering effective operators one by one, but at the expense of the generality of the conclusions. Many models can be analyzed using the effective Lagrangian of Eq. (36), but others introduce new operators and must be treated individually. The list of models considered is not exhaustive, but rather illustrates the new physics reach of NuSOnG.

1. Z' models

Massive Z' fields are one of the simplest signatures of physics beyond the Standard Model. (For a recent review, see [52].) Z' vector bosons are generic in grand unified theories and prevalent in theories that address the electroweak gauge hierarchy. They may stabilize the weak scale directly by canceling off quadratic divergences of Standard Model fields, as in theories of extra-dimensions or Little Higgs theories. In supersymmetric models, Z' fields are not needed to cancel quadratic divergences, but are still often tied to the scale of soft-breaking (and hence the electroweak scale). In these last two cases, the Z' typically has a TeV-scale mass, and is an attractive target for NuSOnG.

If the Z' mass is sufficiently large, its exchange is well-described at NuSOnG energies by the effective operator of Eq. (43). In this case, the new physics scale is related to the Z' model by $\Lambda \sim M_{Z'}/g_{Z'}$, the ratio of the Z' mass to its gauge-coupling. Further model-dependence shows up in the ratio of fermion charges under the U(1)$'$ symmetry associated with the Z', and the presence of any $Z-Z'$ mixing. With reasonable theoretical assumptions, the absence of new sources of large flavor-changing neutral currents, the consistency of Yukawa interactions, and anomaly cancellation with a minimal number of exotic fermions, the number of interesting models can be reduced substantially, to four discrete families of generic $U(1)'$ models each containing one free parameter, x [53]. In Table V A 1, we indicate the charges of $\nu_{\mu L}, e_L, e_R$ under these families of $U(1)'$ symmetries.

Using the sensitivity of NuSOnG to the scale Λ in ν_μ scattering shown in Figure 9, we can bound the combination $M_{Z'}/g_{Z'}$ for the four families of Z' models as a function of x. It is important to note that these bounds are competitive with the LEP-II bounds found in [53], which are based on Z' decays to all fermions, not just electrons and neutrinos.

There are Z' models which distinguish among generations can affect neutrino scattering. These will be probed

	$U(1)_{B-xL}$	$U(1)_{q+xu}$	$U(1)_{10+x\bar{5}}$	$U(1)_{d-xu}$
$\nu_{\mu L}, e_L$	$-x$	-1	$x/3$	$(-1+x)/3$
e_R	$-x$	$-(2+x)/3$	$-1/3$	$x/3$

TABLE VII: Charges of $\nu_{\mu L}, e_L, e_R$ under 4 phenomenologically viable classes of $U(1)'$ symmetries. Each value of x corresponds to a different $U(1)'$ symmetry that is considered.

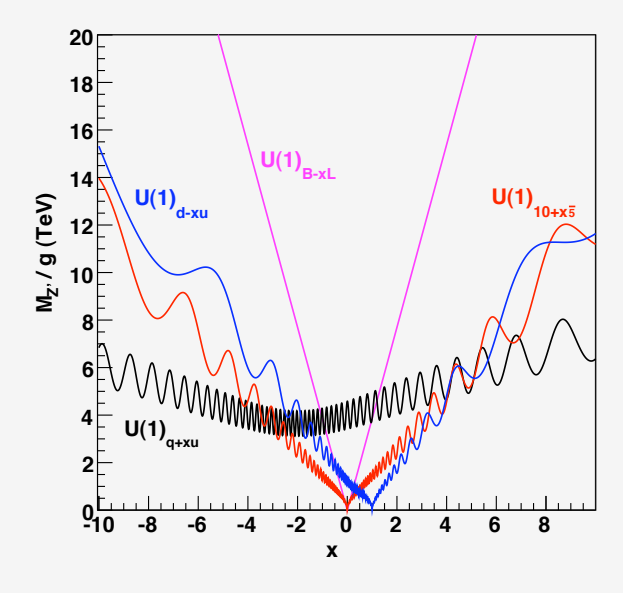

FIG. 13: 95% confidence level sensitivity of NuSOnG to the indicated Z' models. The charges of the electrons and neutrinos under the underlying $U(1)'$ gauge symmetry are described in Table V A 1. The bounds are plotted as functions of the parameter x, which scans over allowed fermion charges for each family of $U(1)'$ symmetries, versus the ratio $M_{z'}/g_{Z'}$.

by NuSOnG at the TeV scale [54, 55, 56, 57, 58]. Among these, $B-3L_\mu$ was suggested as a possible explanation for the NuTeV anomaly [59, 60], however, we show here that this is not the case. Nevertheless, it remains an interesting example to consider.

In the gauged $B-3L_\mu$ the Z' modifies $\nu_\mu N$ DIS. The exchange of the Z' between the ν_μ and the quarks induces operators with coefficients

$$\begin{aligned} \varepsilon^{uL}_{\mu\mu} &= \varepsilon^{uR}_{\mu\mu} = \varepsilon^{dL}_{\mu\mu} = \varepsilon^{dR}_{\mu\mu} \\ &= -\frac{1}{2\sqrt{2}G_F}\frac{g^2_{Z'}}{M^2_{Z'}} \equiv \varepsilon_{B-3L_\mu} . \end{aligned} \tag{58}$$

which shift g^2_L and g^2_R by

$$\Delta g^2_L = \Delta g^2_R = -\frac{2s^2}{3}\varepsilon_{B-3L_\mu}. \tag{59}$$

It should be noted that since ε_{B-3L_μ} is negative, this shows that both g^2_L and g^2_R will be shifted positive. This, in fact, excludes gauged $B-3L_\mu$ as an explanation of the NuTeV anomaly. With this said, a NuSOnG measurement of g^2_L and g^2_R that improves on NuTeV errors by a factor of 2 yields a 2σ bound

$$\frac{M_{Z'}}{g_{Z'}} > 2.2\,\text{TeV} . \tag{60}$$

which is comparable and complementary to the existing bound from D0, and thus interesting to consider.

2. *Models with extended Higgs sectors*

In the Zee [61] and Babu-Zee [62] models, an isosinglet scalar h^+ with hypercharge $Y=+1$ is introduced, which couples to left-handed lepton doublets ℓ as

$$\mathcal{L}_h = \lambda_{ab}\left(\overline{\ell^c_{aL}}\, i\sigma_2\, \ell_{bL}\right) h^+ + h.c. , \tag{61}$$

where (ab) are flavor indices: $a,b = e,\mu,\tau$. The exchange of a charged Higgs induces the effective operator from Eq. (36) which with coefficient

$$\varepsilon^{eL}_{\mu\mu} = -\frac{1}{\sqrt{2}G_F}\frac{|\lambda_{e\mu}|^2}{M^2_h} , \qquad \varepsilon^{eR}_{\mu\mu} = 0 . \tag{62}$$

From Eq. (42), the 95% bound is:

$$\frac{M_h}{|\lambda_{e\mu}|} > 5.2\,\text{TeV}, . \tag{63}$$

competitive with current bound from τ-decay of 5.4 TeV.

3. *R-parity violating SUSY*

Assuming the particle content of the Minimal Supersymmetric Standard Model (MSSM), the most general R-parity violating superpotential (involving only tri-linear couplings) has the form [63]

$$W_{\not R} = \frac{1}{2}\lambda_{ijk}\hat{L}_i\hat{L}_j\hat{E}_k + \lambda'_{ijk}\hat{L}_i\hat{Q}_j\hat{D}_k + \frac{1}{2}\lambda''_{ijk}\hat{U}_i\hat{D}_j\hat{D}_k , \tag{64}$$

where $\hat{L}_i$, $\hat{E}_i$, $\hat{Q}_i$, $\hat{D}_i$, and $\hat{U}_i$ are the left-handed MSSM superfields defined in the usual fashion, and the subscripts $i,j,k = 1,2,3$ are the generation indices. $SU(2)_L$ gauge invariance requires the couplings λ_{ijk} to be anti-symmetric in the first two indices:

$$\lambda_{ijk} = -\lambda_{jik} , \tag{65}$$

The purely baryonic operator $\hat{U}_i\hat{D}_j\hat{D}_k$ is irrelevant to neutrino scattering, so only the 9 λ_{ijk} and 27 λ'_{ijk} couplings are of interest.

From the $\hat{L}\hat{L}\hat{E}$ part of the Eq. (64) slepton exchange will contribute to $\nu_\mu e$ ES at NuSOnG. These induce four-fermion operators appearing in Eq. (36) with corresponding coefficients

$$\varepsilon^{eL}_{\mu\mu} = -\frac{1}{4\sqrt{2}G_F}\sum_{k=1}^{3}\frac{|\lambda_{21k}|^2}{M^2_{\tilde{e}_{kR}}} ,$$

Coupling	95% NuSOnG bound	current 95% bound
$\|\lambda_{121}\|$	0.03	0.05 (V_{ud})
$\|\lambda_{122}\|$	0.04	0.05 (V_{ud})
$\|\lambda_{123}\|$	0.04	0.05 (V_{ud})
$\|\lambda_{231}\|$	0.05	0.07 (τ decay)
$\|\lambda'_{211}\|$	0.05	0.06 (π decay)
$\|\lambda'_{212}\|$	0.06	0.06 (π decay)
$\|\lambda'_{213}\|$	0.06	0.06 (π decay)
$\|\lambda'_{221}\|$	0.07	0.21 (D meson decay)
$\|\lambda'_{231}\|$	0.07	0.45 ($Z \to \mu^+\mu^-$)

TABLE VIII: Potential bounds on the R-parity violating LLE (top) and LQD (bottom) couplings from NuSOnG, assuming that only one coupling is non-zero at a time for each set. All squark and slepton masses are set to 100 GeV. To obtain limits for different masses, rescale by $\left(\frac{M}{100\,\mathrm{GeV}}\right)$. Current bounds are from Ref. [64].

$$\varepsilon^{eR}_{\mu\mu} \;=\; +\frac{1}{4\sqrt{2}G_F}\sum_{j=1,3}\frac{|\lambda_{2j1}|^2}{M^2_{\tilde{e}_{jL}}}\,. \qquad (66)$$

If we place bounds on the sleptons one at a time, then Eq. (42) translates to the 2σ bounds shown in Table VIII, presented for masses of 100 GeV. To rescale to different masses, use $\left(\frac{M}{100\,\mathrm{GeV}}\right)$. This can be compared to current bounds Ref. [64]. NuSOnG improves all of these bounds.

From the $\hat{L}\hat{Q}\hat{D}$ part of Eq. (64), squark exchange will contribute to contribute to NC $\nu_\mu N$ DIS and CC $\nu_\mu N$ DIS. The resulting shifts in g^2_L and g^2_R are

$$\begin{aligned}\delta g^2_L &= 2\Big[\, g^{\nu d}_L \varepsilon^{dL}_{\mu\mu} - g^2_L \varepsilon_c \,\Big]\,,\\ \delta g^2_R &= 2\Big[\, g^{\nu d}_R \varepsilon^{dR}_{\mu\mu} - g^2_R \varepsilon_c \,\Big]\,, \end{aligned} \qquad (67)$$

where

$$\begin{aligned}\varepsilon^{dL}_{\mu\mu} &= -\frac{1}{4\sqrt{2}G_F}\sum_{k=1}^{3}\frac{|\lambda'_{21k}|^2}{M^2_{\tilde{d}_{kR}}}\,,\\ \varepsilon^{dR}_{\mu\mu} &= -\frac{1}{4\sqrt{2}G_F}\sum_{j=1}^{3}\frac{|\lambda'_{2j1}|^2}{M^2_{\tilde{d}_{jL}}}\,,\\ \varepsilon_c &= +\frac{1}{4\sqrt{2}G_F}\sum_{k=1}^{3}\frac{|\lambda'_{21k}|^2}{M^2_{\tilde{d}_{kR}}} \;=\; -\varepsilon^{dL}_{\mu\mu}\,, \end{aligned} \qquad (68)$$

$\varepsilon^{dL}_{\mu\mu}$ and $\varepsilon^{dR}_{\mu\mu}$ are associated with terms of Eq. (36), while ε_c is associated with a four-fermion interaction that corrects charged currents,

$$-2\sqrt{2}G_F\varepsilon_c\Big[\big(\overline{\mu_L}\gamma_\sigma\nu_{\mu L}\big)\big(\overline{u_L}\gamma^\sigma d_L\big) + h.c.\,\Big]\,. \qquad (69)$$

The shifts in g^2_L and g^2_R are:

$$\begin{aligned}\delta g^2_L &= 2\left(g^{\nu d}_L + g^2_L\right)\varepsilon^{dL}_{\mu\mu}\,,\\ \delta g^2_R &= 2g^2_R\varepsilon^{dL}_{\mu\mu} + 2g^{\nu d}_R\varepsilon^{dR}_{\mu\mu}\,. \end{aligned} \qquad (70)$$

Assuming the projected precision goals for NuSOnG on g^2_L and g^2_R, and allowing only one of the couplings to be nonozero at a time, the 2σ bounds are given in Table VIII mass of 100 GeV, in all cases. To obtain limits for different masses, one simply rescales by $\left(\frac{M}{100\,\mathrm{GeV}}\right)$. NuSOnG's measurements are competitive with π decay bounds, and improves the current bounds on the 221 and 231 couplings by factors of 3 and 5, respectively.

4. *Intergenerational leptoquark models*

Measurements of g^2_L and g^2_R are sensitive to leptoquarks. Because the exchange of a leptoquark can interfere with both W and Z exchange processes, we cannot use the limits on the NSI's of Eq. (36), since we must also include the effects of the four-fermion operators associated with charged-current processes. Instead, the interactions of leptoquarks with ordinary matter can be described in a model-independent fashion by an effective low-energy Lagrangian as discussed in Refs. [65, 66] for generation-universal leptoquark couplings. For leptoquarks to contribute to $\nu_\mu N$ DIS, they must couple second generation leptons to first generation quarks, so we use the more general Lagrangian of [67, 68], which allows the coupling constants to depend on the generations of the quarks and leptons that couple to each leptoquark. We summarize the quantum numbers and couplings of the various leptoquarks fields in Table IX; our notation conventions are those of Ref. [68].

The four-fermion operators induced by leptoquark exchange will affect NC and/or CC processes, and at NuSOnG the effect manifests itself in shifts g^2_L and g^2_R. Assuming degenerate masses within each iso-multiplet, the shifts in g^2_L and g^2_R can be written generically as

$$\begin{aligned}\delta g^2_L &= C_L\,\frac{|\lambda^{12}_{LQ}|^2/M^2_{LQ}}{g^2/M^2_W} \;=\; \frac{C_L}{4\sqrt{2}G_F}\frac{|\lambda^{12}_{LQ}|^2}{M^2_{LQ}}\,,\\ \delta g^2_R &= C_R\,\frac{|\lambda^{12}_{LQ}|^2/M^2_{LQ}}{g^2/M^2_W} \;=\; \frac{C_R}{4\sqrt{2}G_F}\frac{|\lambda^{12}_{LQ}|^2}{M^2_{LQ}}\,, \end{aligned} \qquad (71)$$

where λ^{12}_{LQ} denotes the $(ij) = (12)$ coupling of the leptoquark and M_{LQ} is its mass. In table X we list what they are, and in figure 14 we plot the dependence of δg^2_L and δg^2_R on the ratio $|\lambda_{LQ}|^2/M^2_{LQ}$. Table X also lists the projected NuSOnG bounds on the coupling constants [69]. Existing bounds on S_1, $\vec{S}_3$, V_1, and $\vec{V}_3$ couplings from $R_\pi = Br(\pi \to e\nu)/Br(\pi \to \mu\nu)$ are already much stronger, but could be circumvented for $\vec{S}_3$ and $\vec{V}_3$ if the masses within the multiplet are allowed to be non-degenerate.

Leptoquark		Spin	F	$SU(3)_C$	I_3	Y	Q_{em}	Allowed Couplings
S_1	S_1^0	0	-2	$\bar{3}$	0	$\frac{1}{3}$	$\frac{1}{3}$	$g_{1L}(\overline{u_L^c}e_L - \overline{d_L^c}\nu_L)$, $g_{1R}(\overline{u_R^c}e_R)$
$\tilde{S}_1$	$\tilde{S}_1^0$	0	-2	$\bar{3}$	0	$\frac{4}{3}$	$\frac{4}{3}$	$\tilde{g}_{1R}(\overline{d_R^c}e_R)$
$V_{2\mu}$	$V_{2\mu}^+$	1	-2	$\bar{3}$	$+\frac{1}{2}$	$\frac{5}{6}$	$\frac{4}{3}$	$g_{2L}(\overline{d_R^c}\gamma^\mu e_L)$, $g_{2R}(\overline{d_L^c}\gamma^\mu e_R)$
	$V_{2\mu}^-$				$-\frac{1}{2}$		$\frac{1}{3}$	$g_{2L}(\overline{d_R^c}\gamma^\mu \nu_L)$, $g_{2R}(\overline{u_L^c}\gamma^\mu e_R)$
$\tilde{V}_{2\mu}$	$\tilde{V}_{2\mu}^+$	1	-2	$\bar{3}$	$+\frac{1}{2}$	$-\frac{1}{6}$	$\frac{1}{3}$	$\tilde{g}_{2L}(\overline{u_R^c}\gamma^\mu e_L)$
	$\tilde{V}_{2\mu}^-$				$-\frac{1}{2}$		$-\frac{2}{3}$	$\tilde{g}_{2L}(\overline{u_R^c}\gamma^\mu \nu_L)$
$\vec{S}_3$	S_3^+	0	-2	$\bar{3}$	$+1$	$\frac{1}{3}$	$\frac{4}{3}$	$-\sqrt{2}g_{3L}(\overline{d_L^c}e_L)$
	S_3^0				0		$\frac{1}{3}$	$-g_{3L}(\overline{u_L^c}e_L + \overline{d_L^c}\nu_L)$
	S_3^-				-1		$-\frac{2}{3}$	$\sqrt{2}g_{3L}(\overline{u_L^c}\nu_L)$
S_2	S_2^+	0	0	3	$+\frac{1}{2}$	$\frac{7}{6}$	$\frac{5}{3}$	$h_{2L}(\overline{u_R}e_L), h_{2R}(\overline{u_L}e_R)$
	S_2^-				$-\frac{1}{2}$		$\frac{2}{3}$	$h_{2L}(\overline{u_R}\nu_L), -h_{2R}(\overline{d_L}e_R)$
$\tilde{S}_2$	$\tilde{S}_2^+$	0	0	3	$+\frac{1}{2}$	$\frac{1}{6}$	$\frac{2}{3}$	$\tilde{h}_{2L}(\overline{d_R}e_L)$
	$\tilde{S}_2^-$				$-\frac{1}{2}$		$-\frac{1}{3}$	$\tilde{h}_{2L}(\overline{d_R}\nu_L)$
$V_{1\mu}$	$V_{1\mu}^0$	1	0	3	0	$\frac{2}{3}$	$\frac{2}{3}$	$h_{1L}(\overline{u_L}\gamma^\mu\nu_L + \overline{d_L}\gamma^\mu e_L)$, $h_{1R}(\overline{d_R}\gamma^\mu e_R)$
$\tilde{V}_{1\mu}$	$\tilde{V}_{1\mu}^0$	1	0	3	0	$\frac{5}{3}$	$\frac{5}{3}$	$\tilde{h}_{1R}(\overline{u_R}\gamma^\mu e_R)$
$\vec{V}_{3\mu}$	$V_{3\mu}^+$	1	0	3	$+1$	$\frac{2}{3}$	$\frac{5}{3}$	$\sqrt{2}h_{3L}(\overline{u_L}\gamma^\mu e_L)$
	$V_{3\mu}^0$				0		$\frac{2}{3}$	$h_{3L}(\overline{u_L}\gamma^\mu\nu_L - \overline{d_L}\gamma^\mu e_L)$
	$V_{3\mu}^-$				-1		$-\frac{1}{3}$	$\sqrt{2}h_{3L}(\overline{d_L}\gamma^\mu\nu_L)$

TABLE IX: Quantum numbers of scalar and vector leptoquarks with $SU(3)_C \times SU(2)_L \times U(1)_Y$ invariant couplings to quark-lepton pairs ($Q_{\rm em} = I_3 + Y$) [11].

LQ	C_L	C_R	$\lvert\lambda_{LQ}\rvert^2$	NuSOnG 95% bound	95% bound from R_π
S_1	$s^2\left(\frac{4}{3} - \frac{10}{9}s^2\right)$	$-\frac{10}{9}s^4$	$\lvert g_{1L}^{12}\rvert^2$	0.0036	0.0037
$\vec{S}_3$	$+\frac{10}{9}s^4$	$+\frac{10}{9}s^4$	$\lvert g_{3L}^{12}\rvert^2$	0.010	0.0008
S_2	0	$-\frac{8}{3}s^2$	$\lvert h_{2L}^{12}\rvert^2$	0.0013	N/A
$\tilde{S}_2$	0	$+\frac{4}{3}s^2$	$\lvert \tilde{h}_{2L}^{12}\rvert^2$	0.0026	N/A
V_1	$s^2\left(\frac{4}{3} - \frac{20}{9}s^2\right)$	$-\frac{20}{9}s^4$	$\lvert h_{1L}^{12}\rvert^2$	0.0040	0.0018
$\vec{V}_3$	$-4s^2\left(1 - \frac{5}{9}s^2\right)$	$+\frac{20}{9}s^4$	$\lvert h_{3L}^{12}\rvert^2$	0.0011	0.0004
V_2	0	$-\frac{4}{3}s^2$	$\lvert g_{2L}^{12}\rvert^2$	0.0026	N/A
$\tilde{V}_2$	0	$+\frac{8}{3}s^2$	$\lvert \tilde{g}_{2L}^{12}\rvert^2$	0.0013	N/A

TABLE X: Potential and existing 95% bounds on the leptoquark couplings squared when the leptoquark masses are set to 100 GeV. To obtain the limits for different leptoquark masses, multiply by $(M_{LQ}/100\,{\rm GeV})^2$. Existing bounds on the S_1, $\vec{S}_3$, V_1, and $\vec{V}_3$ couplings from $R_\pi = Br(\pi \to e\nu)/Br(\pi \to \mu\nu)$ are also shown.

B. Interplay with LHC to Isolate the Source of New Physics

By the time NuSOnG runs, the LHC will have accumulated a wealth of data and will have begun to change the particle physics landscape. The message from LHC data may be difficult to decipher, however. As discussed below, NuSOnG will be able to help elucidate the new physics revealed at the LHC. The discovery of a Higgs along with the anticipated measurement of the top mass to 1 GeV precision would effectively fix the center of the ST plot and will enhance the power of the precision electroweak data as a tool for discovering new physics. If additional resonances are discovered at the LHC, it is still likely that little will be learned about their couplings.

The NuSOnG experiment provides complementary information to LHC. Rather than generalize, to illustrate the power of NuSOnG, two specific examples are given here. We emphasize that these are just two of a wide range of examples, but they serve well to demonstrate the point. Here we have chosen examples from typical new physics models other than Z' models which were discussed above, in order to demonstrate the physics range which can be probed by NuSOnG.

First, extend the Standard Model to include a non-degenerate $SU(2)_L$ triplet leptoquark ($\vec{S}_3$ or $\vec{V}_3$ in the notation of [65], with masses in the 0.5-1.5 TeV range. At the LHC these leptoquarks will be produced primarily in pairs through gluon fusion, and each leptoquark will decay to a lepton and a jet [75]. The peak in the lepton-jet invariant mass distribution will be easily detected over background. This will provide the leptoquark masses but yield little information about their couplings to fermions. The leptoquarks will also shift the neutrino-nucleon effective coupling g_L^2 in a way that depends sensitively on both the leptoquark couplings and masses. Such

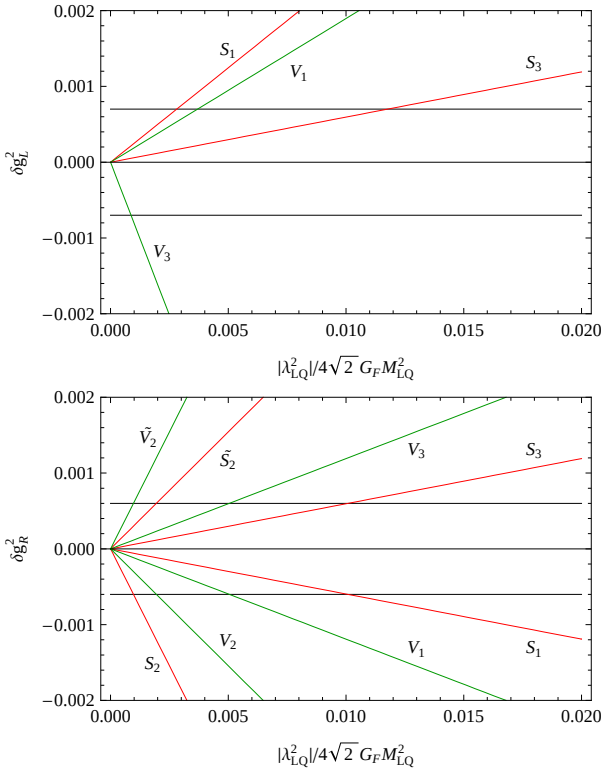

FIG. 14: Shifts in g_L^2 and g_R^2 due to leptoquarks. Horizontal lines indicate the projected 1σ limits of NuSOnG.

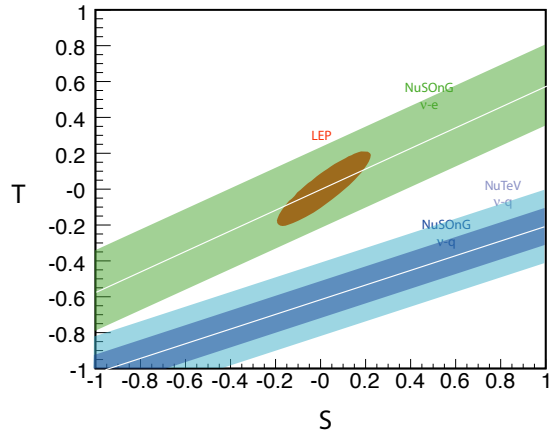

FIG. 15: NuSOnG expectation in the case of a Tev-scale triplet leptoquark. For clarity, this plot and the two following cases, show the expectation from only the two highest precision measurements from NuSOnG: g_L^2 and ν ES.

a leptoquark-induced shift could provide an explanation for the NuTeV anomaly [60, 67, 76]. In this scenario, NuSOnG would find that isospin and the strange sea can be constrained to the point that they do not provide an explanation for the NuTeV anomaly, thus the NuTeV anomaly is the result of new physics. The NuSOnG PW measurement of $\sin 2\theta_W$ will agree with NuTeV; g_R^2 and

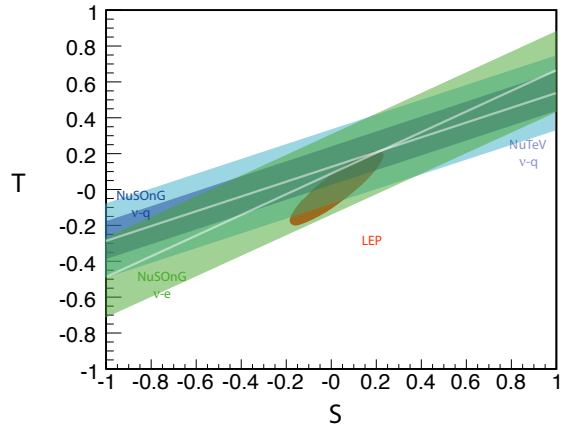

FIG. 16: NuSOnG expectation if the NuTeV anomaly is due to isospin violation and there is a heavy 4th generation with isospin violation.

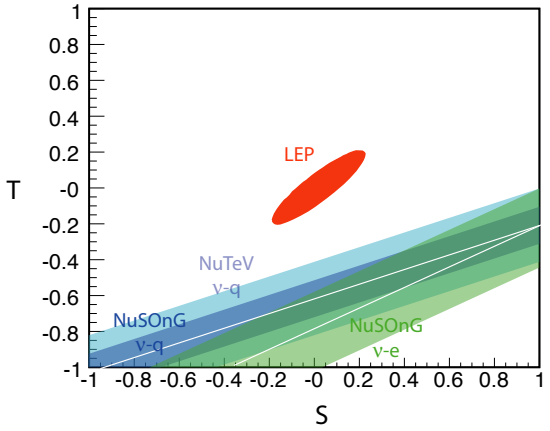

FIG. 17: If LHC sees a Standard Model Higgs and no evidence of new physics, NuSOnG may reveal new physics in the neutrino sector.

the νe and $\overline{\nu} e$ elastic scattering measurements will agree with LEP. Fig. 15 illustrates this example. NuSOnG's measurement of g_L^2 would provide a sensitive measurement of the leptoquark couplings when combined with the LHC mass measurements as inputs.

A second example is the existence of a fourth generation family. A fourth family with non-degenerate masses (*i.e.* isospin violating) is allowed within the LEP/SLD constraints [78]. As a model, we choose a fourth family with mass splitting on the order of $\sim$ 75 GeV and a 300 GeV Higgs. This is consistent with LEP at 1σ and perfectly consistent with M_W, describing the point (0.2,0.19) on the ST plot. In this scenario, LHC will measure the Higgs mass from the highly enhanced $H \to ZZ$ decay. An array of exotic decays which will be difficult to fully reconstruct, such as production of 6 W's and 2 b's, will be observed at low rates. In this scenario, isospin violation explains the NuTeV anomaly, thus the NuTeV

PW and the NuSOnG PW measurements agree with the νeES measurements. These three precision neutrino results, all with "LEP-size" errors, can be combined and will intersect the one-sigma edge of the LEP measurements. Fig. 16 illustrates this example. From this, the source, a fourth generation with isospin violation, can be demonstrated.

Lastly, while it seems unlikely, it is possible that LHC will observe a Standard Model Higgs and no signatures of new physics. If this is the case, it is still possible for NuSOnG to add valuable clues to new physics. This is because the experiment is uniquely sensitive to the neutrino sector. If a situation such as is illustrated on Fig. 17 arose, the only explanation would be new physics unique to neutrino interactions.

VI. IMPACT OF QCD MEASUREMENTS

An important aspect of NuSOnG is that new physics can be probed through both ES and DIS. The ES measurement is a theoretically robust, purely leptonic measurement. On the other hand, as discussed above, the DIS measurement requires knowledge of PDFs which describe the momentum distribution of quarks as a function of Q^2. This can bring in theoretical uncertainties from sources such as nuclear effects and nuclear isospin violation.

These uncertainties can be addressed by making a high statistics measurement of the PDFs on glass, *in situ*. The experiment will generate an unprecedented sample of >100M DIS events which can be used to measure six structure functions (three on neutrinos and three on antineutrinos) as well as the strange and anti-strange parton distributions. These PDFs provide the input to the simulation in the PW-style analysis from which the electroweak parameters are extracted. This "internally self-consistent analysis technique" [24] was employed by the NuTeV experiment; however the statistics were limited and external data were also used as input. NuSOnG should have sufficient data to do a fully self-consistent analysis.

In this article, we confine the QCD discussion to the measurements which impact the electroweak analyses. However, we note that the physics of QCD measurements of NuSOnG is interesting in its own right. Unfortunately, the scope of the NuSOnG QCD program extends beyond the discussion presented here.

In the subsections below, the QCD measurements are described. We then consider the three main QCD issues for the electroweak PW analysis and discuss both the constraints from our measurements and cross checks from external sources.

Experiment	ν DIS events	$\bar{\nu}$ DIS events	main target	isoscalar correction
CCFR	0.95M	0.17M	iron	5.67% [79]
NuTeV	0.86M	0.24M	iron	5.74% [80]
NuSOnG	606M	34M	glass	isoscalar

TABLE XI: Comparison of statistics and targets for parton distribution studies in NuSOnG compared to the two past highest statistics DIS neutrino scattering experiments.

A. Deep Inelastic Scattering and Parton Distribution Functions

Obtaining a high quality model of the parton distribution functions in neutrino and antineutrino scattering is crucial to the NuSOnG electroweak PW measurement. NuSOnG will go a step beyond past experiments in addressing the systematics of parton distribution functions (PDFs) by making high statistics measurements for neutrino and antineutrino data separately. Table XI shows the large improvement in statistics for NuSOnG compared to NuTeV and CCFR, the previous highest statistics experiments. Issues of uncertainties on the nuclear corrections are avoided by extracting PDFs on SiO_2 directly, in similar fashion to the NuTeV PW analysis.

The differential cross sections for neutrino and antineutrino CC DIS each depend on three structure functions: F_2, xF_3 and R_L. They are given by:

$$\frac{d^2\sigma^{\nu(\overline{\nu})N}}{dxdy} = \frac{G_F^2 M E_\nu}{\pi\left(1+Q^2/M_W^2\right)^2}\left[F_2^{\nu(\overline{\nu})N}(x,Q^2)\left(\frac{y^2+(2Mxy/Q)^2}{2+2R_L^{\nu(\overline{\nu})N}(x,Q^2)}+1-y-\frac{Mxy}{2E_\nu}\right)\pm xF_3^{\nu(\overline{\nu})N}y\left(1-\frac{y}{2}\right)\right] \quad (72)$$

where $+(-)$ is for $\nu(\overline{\nu})$ scattering. In this equation, x is the Bjorken scaling variable, y the inelasticity, and Q^2 the squared four-momentum transfer. The structure functions are directly related to the PDFs.

The function $xF_3(x,Q^2)$ is unique to the DIS cross section for the weak interaction. It originates from the parity-violating term in the product of the leptonic and hadronic tensors. For an isoscalar target, in the quark-parton model, where $s=\bar{s}$ and $c=\bar{c}$,

$$xF_3^{\nu N}(x) = x\left(u(x)+d(x)+2s(x)-\bar{u}(x)-\bar{d}(x)-2\bar{c}(x)\right), \quad (73)$$

$$xF_3^{\bar{\nu}N}(x) = xF_3^{\nu N}(x)-4x\left(s(x)-c(x)\right). \quad (74)$$

In past experiments, the average of xF_3 for neutrinos and antineutrinos has been measured. Defining $xF_3 =$

$\frac{1}{2}(xF_3^{\nu N} + xF_3^{\bar{\nu} N})$, at leading order in QCD,

$$xF_{3,LO} = \sum_{i=u,d..} xq_i(x,Q^2) - x\overline{q_i}(x,Q^2). \qquad (75)$$

To the level that the sea quark distributions have the same x dependence, and thus cancel, xF_3 can be thought of as probing the valence quark distributions. The difference between the neutrino and antineutrino parity violating structure functions, $\Delta(xF_3) = xF_3^{\nu N} - xF_3^{\bar{\nu} N}$, probes the strange and charm seas.

The function $F_2(x,Q^2)$ appears in both the cross section for charged lepton (e or μ) DIS and the cross section for ν DIS. At leading order,

$$F_{2,LO} = \sum_{i=u,d..} e_i^2(xq_i(x,Q^2) + x\overline{q_i}(x,Q^2)), \qquad (76)$$

where e_i is the charge associated with the interaction. In the weak interaction, this charge is unity. For charged-lepton scattering mediated by a virtual photon, e_i is the fractional electromagnetic charge of the quark flavor. Thus $F_2^{\nu N}$ and $F_2^{e(\mu)N}$ are analogous but not identical and comparison yields useful information about specific parton distributions [81] and charge symmetry violation as discussed below. In past neutrino experiments, F_2^{ν} and $F_2^{\bar{\nu}}$ have been taken to be identical and an average F_2 has been extracted, although this is not necessarily true in nuclear targets, as discussed below.

Similarly, $R_L(x,Q^2)$, the longitudinal to transverse virtual boson absorption cross-section ratio, appears in both the charged-lepton and neutrino scattering cross sections. To extract R_L from the cross section, one must bin in x,Q^2 and y. This requires a very large data set. To date, the best measurements for this come from charged lepton scattering rather than neutrino scattering [82]. Therefore, neutrino experiments have used charged lepton fits to R_L as an input to the measurements of xF_3 and F_2 [83]. This, however, is just a matter of the statistics needed for a global fit to all of the unknown structure functions in x and Q^2 bins [84]. With the high statistics of NuSOnG, precise measurement of R_L will be possible from neutrino scattering for the first time.

As an improvement on past experiments, the high statistics of NuSOnG allows measurement of all six structure functions: F_2^{ν}, $F_2^{\bar{\nu}}$, xF_3^{ν}, $xF_3^{\bar{\nu}}$, R_L^{ν} and $R_L^{\bar{\nu}}$. This is done by fitting the neutrino and antineutrino data separately in x, y and Q^2 as described in Eq. (72). The first steps toward fitting all six structure functions independently were made by the CCFR experiment [85], however statistics were such that only xF_3^{ν}, $xF_3^{\bar{\nu}}$, and F_2-average and R-average could be measured, where the average is over ν and $\bar{\nu}$. A global fit to the six structure functions in NuSOnG allows separate parameterizations of the underlying PDFs which can account for the nuclear and isospin violation issues discussed below.

In addition to fitting to the inclusive DIS sample, neutrino scattering can also probe parton distributions through exclusive samples. A unique and important case is the measurement of the strange sea through opposite sign dimuon production. When the neutrino interacts with an s or d quark, it produces a charm quark that fragments into a charmed hadron. The charmed hadron's semi-leptonic decay (with branching ratio $B_c \sim 10\%$) produces a second muon of opposite sign from the first:

$$\nu_\mu + \mathrm{N} \longrightarrow \mu^- + c + \mathrm{X} \qquad (77)$$
$$\hookrightarrow s + \mu^+ + \nu_\mu. \qquad (78)$$

Similarly, with antineutrinos, the interaction is with an $\overline{s}$ or $\overline{d}$,

$$\overline{\nu}_\mu + \mathrm{N} \longrightarrow \mu^+ + \overline{c} + \mathrm{X}$$
$$\hookrightarrow \overline{s} + \mu^- + \overline{\nu}_\mu. \qquad (79)$$

The opposite sign of the two muons can be determined for those events where both muons reach the toroid spectrometer. Study of these events as a function of the kinematic variables allows extraction of the strange sea, the charm quark mass, the charmed particle branching ratio (B_c), and the Cabibbo-Kobayashi-Maskaka matrix element, $|V_{cd}|$.

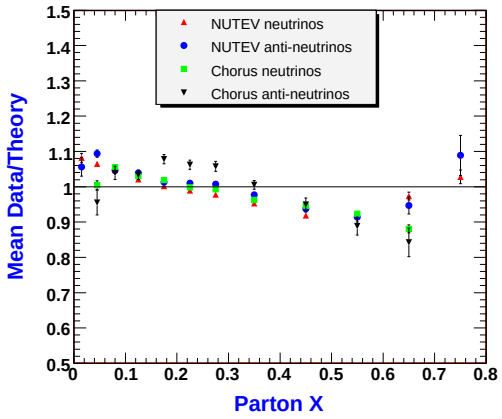

FIG. 18: Comparison between the reference fit and the unshifted CHORUS and NuTeV neutrino data without any nuclear corrections.

B. Nuclear Effects

The NuSOnG target is SiO_2. In principle, parton distribution measurements from other targets (other A, deuterium and protons) and using the charged leptons (e, μ) can be used to parametrize the underlying quark physics. While theoretical models have been developed [86, 87], it has been difficult to find a common parameterization which describes all of the data [88]. Fig. 18 shows some results from Ref. [89] in the form of "data/theory" averaged over Q^2 and presented versus x. The results are from a global fit but are plotted *without* the model-dependent nuclear corrections which were used in the fits.

It is notable that the overall pattern of deviations shown in Fig. 18 are, in general, similar to that seen in charged lepton DIS [88]. However, the deviations from unity are perhaps smaller. At high x, the effect of Fermi smearing is clear. At moderate x the EMC effect is observable. It is interesting to note that there is no clear indication of the turnover at low x which is observed in charged lepton scattering, called shadowing. This may be due to kinematic limits of the measurements, which NuSOnG can extend.

Also, note the striking similarity between the ν and $\overline{\nu}$ results. This appears to imply that the differences in the nuclear effects between neutrino and antineutrino DIS is small. As discussed later, when we consider ΔxF_3 and isospin violation, it is crucial to model differences in the nuclear effects between ν and $\bar{\nu}$ scattering as a function of x. Such effects can be constrained by the comparison of the F_2^{ν} and $F_2^{\bar{\nu}}$ data and will be implicitly included in PDF fits which are done to the neutrino and antineutrino data separately.

While the general description fits the data, the results are not in sufficient agreement for the stringent requirements of a 0.4% measurement of $\sin^2\theta_W$ [87]. Instead, NuSOnG will measure the parton distributions on glass to high precision. Nuclear effects are thereby directly incorporated into the model, without any external inputs. Looking beyond the electroweak results, these measurements will be quite interesting for addressing the issues with nuclear effects raised by Fig. 18.

C. Measurement of the Strange Sea

Charged current neutrino-induced charm production, $(\nu/\bar{\nu})N \to \mu^+\mu^- X$, proceeds primarily through the subprocesses $W^+ s \to c$ and $W^- \bar{s} \to \bar{c}$ (respectively), so this provides a unique mechanism to directly probe the $s(x)$ and $\bar{s}(x)$ distributions. Approximately 10% of the time the charmed particles decay into $\mu + X$, adding a second oppositely signed muon to the CC event's final state. These "dimuon" events are easily distinguishable, and make up approximately 1% of the total CC event sample. Hence, the recent high-statistics dimuon measurements [90, 91, 92, 93, 94] play an essential role in constraining the strange and anti-strange components of the proton. On NuSOnG, the dimuon data will be used in the same manner.

Distinguishing the difference between the $s(x)$ and $\bar{s}(x)$ distributions,

$$xs^-(x) \equiv xs(x) - x\bar{s}(x), \tag{80}$$

is necessary for the PW style analysis. This analysis is sensitive to the integrated strange sea asymmetry,

$$S^- \equiv \int_0^1 s^-(x)dx, \tag{81}$$

through its effect on the denominator of the PW ratio, as has been recognized in numerous references [60, 95, 96, 97, 98]).

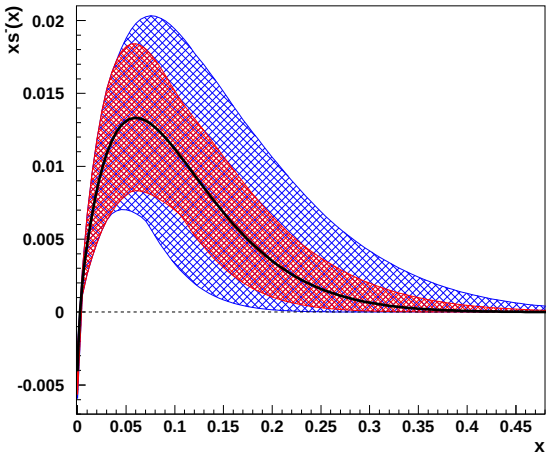

FIG. 19: NuTeV measurement of $xs^-(x)$ vs x at $Q^2 = 16$ GeV^2. Outer band is combined errors, inner band is without B_c uncertainty.

The highest precision study of s^- to date is from the NuTeV experiment [32]. The sign selected beam allowed measurement of the strange and anti-strange seas independently, recording 5163 neutrino-induced dimuons, and 1380 antineutrino-induced dimuon events in its iron target. Figure 19 shows the fit for asymmetry between the strange and anti-strange seas in the NuTeV data.

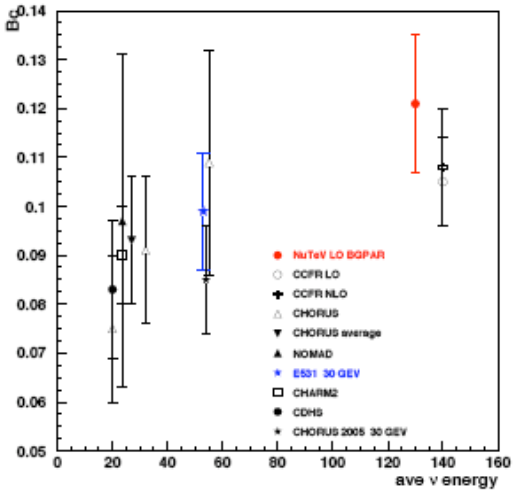

FIG. 20: World measurements of B_c. See refs. [99] through [104].

The integrated strange sea asymmetry from NuTeV has a positive central value: 0.00196 ± 0.00046 (stat) ± 0.00045 (syst) $^{+0.00148}_{-0.00107}$ (external). In NuSOnG, as in NuTeV, the statistical error will be dominated by the antineutrino data set and is expected to be about 0.0002. The systematic error is dominated by the π and K decay-in-flight subtraction. This can be addressed in NuSOnG through testbeam measurements which will allow a more accurate modeling of this background, as well as applying the techniques of CCFR to constrain this rate [105, 106, 107]. We expect to be able to reduce this error to about 0.0002. The combination of these reduces the total error by about 10%, because the main contributon comes from the external inputs.

The external error on the measurement is dominated by the error on the average charm semi-muonic branching ratio, B_c:

$$B_c = \Sigma_i \int \phi(E) f_i(E) B_{\mu - i} dE, \tag{82}$$

where ϕ is the neutrino flux in energy bins, f_i is the energy dependent production fraction for each hadron, and $B_{\mu-i}$ is the semi-muonic branching ratio for each hadron. In the NuTeV analysis, this is an external input, with an error of about 10%. To make further progress, this error must be reduced.

Fig. 20 shows the world measurements of B_c, taken from references [99] through [104]. Measuring B_c directly requires the capability to resolve the individual charmed particles created in the interaction. The best direct measurements are from emulsion. This kind of measurement has been performed in past experiments (E531, Chorus) using emulsion detectors [100, 102], where the decay of the charmed meson is well tagged. Since the cross section for charmed meson production is energy dependent, it is important to make a measurement near the energy range of interest. The NuTeV strange sea asymmetry study used a re-analysis of 125 charm events measured by the FNAL E531 experiment [102] in the energy range of the NuTeV analysis ($E_\nu > 20$ GeV). B_c has also been constrained through indirect measurement via fits.

For NuSOnG, our goal is to reduce the error on B_c using an *in situ* measurement on glass by at least a factor of 1.5. One method is to include B_c as a fit parameter in the analysis of the dimuon data. The unprecedentedly high statistics will allow a fit as a function of neutrino energy for the first time. Dimuons from high x neutrino DIS almost exclusively result from scattering off valence quarks, such that the dimuon cross section in that region isolates B_c from the strange sea. In dimuon fits, the assumption is then taken that $B_{c-\nu} = B_{c-\bar{\nu}}$, B_c may be measured directly from the dimuon data.

Unfortunately, antineutrino charm production is not well measured by past experiments. This leads to concerns about the assumption that $B_{c-\nu} = B_{c-\bar{\nu}}$. An example of a potential source of difference in neutrino and antineutrino mode, consider that $\nu n \to \mu^- \Lambda_c$ has no analogous reaction in the antineutrino channel.

These arguments provide the motivation for including a high resolution target/tracker in the NuSOnG design that can directly measure the semileptonic branching ratio to charm in both ν and $\bar{\nu}$ running modes. There are two feasible detector technologies. The first is to use emulsion, as in past experiments. This is proven technology and scanning could be done at the facility in Nagoya, Japan. The second is to use the NOMAD-STAR detector [10] or a similar detector. This is a 45 kg silicon vertex detector which ran in front of the NOMAD experiment. The target was boron carbide interleaved with the silicon. This detector successfully measured 45 charm events in that beam, identifying D^+, D^0 and D_s. A similar detector of this size in the NuSOnG beam would yield about 900 ν events and 300 $\bar{\nu}$ events. This has the advantage of being a low-Z material which is isoscalar and close in mass to the SiO_2 of the detector.

D. Isospin (Charge Symmetry) Violation and ΔxF_3

The question of isospin violation is central to the PW electroweak measurement. In the NuTeV analysis, isospin symmetry was assumed. As discussed above, various models which admit isospin violation can pull the NuTeV result toward the Standard Model. However it would take significantly larger isospin violation to bring NuTeV into agreement with the data. Better constraint of isospin violation will be crucial to the interpretation of the NuSOnG results.

When we relate DIS measurements from heavy targets such as $^{56}_{26}$Fe (used in NuTeV) or $^{207}_{82}$Pb (Chorus) back to a proton or isoscalar target, we generally make use of isospin symmetry where we assume that the proton and neutron PDFs can be related via a $u \leftrightarrow d$ interchange. While isospin symmetry is elegant and well motivated, the validity of this exact charge symmetry must ultimately be established by experimental measurement. There have been a number of studies investigating isospin symmetry violation [108, 109, 110, 111, 112, 113, 114]; therefore, it is important to be aware of the magnitude of potential violations of isospin symmetry and the consequences on the extracted PDF components. For example, the naive parton model relations are modified if we have a violation of exact $p \leftrightarrow n$ isospin-symmetry, or charge symmetry violation (CSV); *e.g.*, $u_n(x) \not\equiv d_p(x)$ and $u_p(x) \not\equiv d_n(x)$.

It is noteworthy that a violation of isospin symmetry is automatically generated once QED effects are taken into account [115, 116, 117]. This is because the photon couples to the up quark distribution $u_p(x)$ differently than to the down quark distribution $d_n(x)$. These terms can be as much as a few percent in the medium x range, see *e.g.* Fig. 1 in Ref. [117].

Combinations of structure functions can be particularly sensitive to isospin violations, and NuSOnG is well suited to measure some of these observables. For example, residual u, d-contributions to $\Delta xF_3 = xF_3^\nu - xF_3^{\bar{\nu}}$

from charge symmetry violation would be amplified due to enhanced valence components $\{u_v(x), d_v(x)\}$, and because the $d \to u$ transitions are not subject to slow-rescaling corrections which suppress the $s \to c$ contribution to $\Delta x F_3$ [110]. Here the ability of NuSOnG to separately measure xF_3^ν and $xF_3^{\bar\nu}$ over a broad kinematic range will provide powerful constraints on the sensitive structure function combination $\Delta x F_3$.

Separately, the measurement of $\Delta F_2 \equiv \frac{5}{18} F_2^{CC}(x,Q^2) - F_2^{NC}(x,Q^2)$ in Charged Current (CC) $W^\pm$ exchange and Neutral Current (NC) γ/Z exchange processes can also constrain CSV [112]; because NuSOnG will measure F_2^{CC} on a variety of targets, this will reduce the systematics associated with the heavy nuclear target corrections thus providing an additional avenue to study CSV.

In the following, we provide a detailed analysis of CSV which also investigates the various experimental systematics associated with each measurement. We shall find it is important to consider all the systematics which impact the various experimental measurements to assess the discriminating power.

1. $\Delta x F_3$ and Isospin Violations

We recall the leading-order relations of the neutrino structure function F_3 on a general nuclear target:

$$\frac{1}{2}F_3^{\nu A}(x) = d_A + s_A - \bar u_A - \bar c_A + ..., \quad (83)$$

$$\frac{1}{2}F_3^{\bar\nu A}(x) = u_A + c_A - \bar d_A - \bar s_A + ... \quad (84)$$

where A represents the nuclear target $A = \{p, n, d, ...\}$, and the "..." represent higher-order contributions and terms from the third generation $\{b, t\}$ quarks. Note that to illustrate the general features of these processes, we use a schematic notation as in Eq. (83) and Eq. (84); for the numerical calculations, the full NLO expressions are employed including mass thresholds, "slow-rescaling" variables, target mass corrections, and CKM elements where appropriate.

For a nuclear target A we can construct $\Delta x F_3^A$ as:

$$\begin{aligned}\Delta x F_3^A &= x F_3^{\nu A} - x F_3^{\bar\nu A} \\ &= 2x\frac{(N-Z)}{A}\left[\left(u_{p/A} - d_{p/A}\right) + \left(\bar u_{p/A} - \bar d_{p/A}\right)\right] + \\ &+ 2x\, s_A^+ - 2x c_A^+ + x\,\frac{2N}{A}\delta I^A + \mathcal{O}(\alpha_S) \end{aligned} \quad (85)$$

where $\mathcal{O}(\alpha_S)$ represents the higher order QCD corrections, and the isospin violations are given by δI^A:

$$\begin{aligned}\delta I^A &= \left(d_{p/A} - u_{n/A}\right) + \left(d_{n/A} - u_{p/A}\right) + \left(\bar d_{p/A} - \bar u_{n/A}\right) + \\ &\left(\bar d_{n/A} - \bar u_{p/A}\right) . \end{aligned} \quad (86)$$

For a flux-weighted linear combination of F_3^ν and $F_3^{\bar\nu}$, terms proportional to the strange quark asymmetry can enter Eq. (85), *cf.* Refs. [108, 112, 113]. For a sign-selected $\nu/\bar\nu$ beam as for NuTeV or NuSOnG, this complication is not necessary. We have defined $s_A^\pm(x) = [s_A(x) \pm \bar s_A(x)]$ and $c_A^\pm(x) = [c_A(x) \pm \bar c_A(x)]$.

In the limit of isospin symmetry, all four terms on the RHS of Eq. (86) vanish individually. For a nuclear isoscalar target, $Z = N = A/2$, we can construct $\Delta x F_3$ from the above:

$$\Delta x F_3 = x F_3^{\nu A} - x F_3^{\bar\nu A} = 2x s_A^+ - 2x c_A^+ + x\,\delta I^A + \mathcal{O}(\alpha_S) . \quad (87)$$

Note in Eq. (85) that for a nuclear target A which is close to isoscalar we have $Z \sim N$ such that the up and down quark terms are suppressed; this is a benefit of the NuSOnG glass (SiO_2) target which is very nearly isoscalar. More specifically, for SiO_2 we have $Z(\mathrm{O}) = 8$, $Z(\mathrm{Si}) = 14$, $m(\mathrm{O}) = 15.994$, $m(\mathrm{Si}) = 28.0855$. Using $A = Z+N$ we have $(N-Z)/A = (A-2Z)/A$ for the prefactor in Eq. (85) which yields $(N-Z)/A \sim -0.000375$ for O and $(N-Z)/A \sim 0.00304$ for Si.

In Eq. (85) the PDFs $\{u_{p/A}, d_{p/A}, ...\}$ represent quark distributions bound in a nucleus A. With a single nuclear target, we can determine the CSV term δI^A for this specific A; measurements on different nuclear targets would be required in order to obtain the A dependence of δI^A if we need to scale to a proton or isoscalar target.

Thus, an extraction of any isospin violation δI^A requires a careful separation of these contributions from the strange, charm, and higher order terms. Theoretical NLO calculations for $\Delta x F_3$ are available; thus the $\mathcal{O}(\alpha_S)$ corrections can be addressed. Additionally, NuSOnG can use the dimuon process ($\nu N \to \mu^+\mu^- X$) to constrain the strange sea.

In conclusion we find that while this is a challenging measurement, NuSOnG's high statistics measurement of $\Delta x F_3$ should provide a window on CSV which is relatively free of large experimental systematics. We emphasize that $\Delta x F_3$ may be extracted from a single target, thereby avoiding the complications of introducing nuclear corrections associated with different targets. This is in contrast to the other measurements discussed below. However, if we desire to rescale the δI^A effects to a different nucleus A, then multiple targets would be required.

2. Measurement of $\Delta F_2 \equiv \frac{5}{18} F_2^{CC}(x,Q^2) - F_2^{NC}(x,Q^2)$

A separate determination of CSV can be achieved using the measurement of F_2 in CC and NC processes via the relation:

$$\begin{aligned}\Delta F_2 &\equiv \frac{5}{18} F_2^{C,AC}(x,Q^2) - F_2^{NC,A}(x,Q^2) \\ &\simeq \frac{1}{6}x\frac{(N-Z)}{A}\left[\left(u_{p/A} - d_{p/A}\right) + \left(\bar u_{p/A} - \bar d_{p/A}\right)\right] \\ &+ \frac{1}{6}x\, s_A^+(x) - \frac{1}{6}x\, c_A^+(x) + \frac{1}{6}x\,\frac{N}{A}\,\delta I^A \\ &+ \mathcal{O}(\alpha_s) \end{aligned} \quad (88)$$

with the definitions:

$$F_2^{CC,A} = \frac{1}{2}\left[F_2^{\nu A} + F_2^{\bar{\nu} A}\right]$$

$$F_2^{NC,A} = F_2^{\ell A}$$

In Eq. (88), the first term is proportional to $(N-Z)/A$ which vanishes for an isoscalar target. The second and third terms are proportional to the heavy quark distributions s_A^+ and c_A^+. The next term is the CSV contribution which is proportional to δI^A given in Eq. (86). It is curious that this has the same form as the CSV contribution for $\Delta x F_3$ of Eq. (85). Finally, the last term represents the higher-order QCD corrections.

While the character of the terms on the LHS of Eq. (87) and Eq. (88) are quite similar, the systematics of measuring ΔF_2 may differ substantially from that of $\Delta x F_3$. For example, the measurement of ΔF_2 requires the subtraction of structure functions from two entirely different experiments. The CC neutrino–nucleon data are extracted from heavy nuclear targets (to accumulate sufficient statistics); as such, these data are generally subject to large nuclear corrections so that the heavy targets can be related to the isoscalar $N = \frac{1}{2}(p+n)$ limit. Conversely, the NC charged-lepton–nucleon process proceeds via the electromagnetic interaction. Therefore sufficient statistics can be obtained for light targets including H and D and no large heavy target corrections are necessary. Therefore, we must use the appropriate nuclear correction factors when we combine F_2^{CC} and F_2^{NC}, and this will introduce a systematic uncertainty.

Separately, the heavy quark production mechanism is different in the CC and NC processes. Specifically, in the CC case we encounter the process $s + W^+ \to c$ where the charm mass threshold kinematics must be implemented. On the other hand, the NC process is $c + \gamma \to c$ which is proportional to the charm sea distribution and has different threshold behavior than the CC process. Even though the charm production process is modeled at NLO, the theoretical uncertainties which this introduces can dominate precision measurements.

3. Other Measurements of CSV

We very briefly survey other measurements of CSV in comparison to the above.

The measurement of the lepton charge asymmetry in W decays from the Tevatron can constrain the up and down quark distributions [118, 119]. In this case, the extraction of CSV constraints is subtle; while isospin symmetry is not needed to relate p and $\bar{p}$, this symmetry is used in the global fit of the PDFs to reduce data on heavy targets to p.

In the limit that all the data in the global analysis were from proton targets, CSV would not enter; hence this limit only arises indirectly from the mix of targets which enter the global fits. At present, while much of the data does come from proton targets (H1, ZEUS, CDF, D0), there are some data sets from both p and d (BCDMS, NMC, E866), and some that use heavier targets (E-605, NuTeV) [120, 121]. Thus, an outstanding question is if CSV were present, to what extent would this be "absorbed" into the the global fit. The ideal procedure would be to parameterize the CSV and include this in the global analysis. While this step has yet to be implemented, there is a recent effort to include the nuclear corrections as a dynamic part of the global fit [88].

Additionally, NMC measures F_2^n/F_2^p data which has an uncertainty of order a few percent [122]. There are also fixed-target Drell-Yan experiments such as NA51 [114] and E866 [123] which are sensitive to the ratio $\bar{d}/\bar{u}$ in the range $0.04 < x < 0.27$. We will soon have LHC data (pp) to add to our collection, thus providing additional constraints in a new kinematic region.

4. Conclusions on Charge Symmetry Violation

NuSOnG will be able to provide high statistics DIS measurements across a wide x range. Because the target material (SiO_2) is nearly isoscalar, this will essentially allow a direct extraction of the isoscalar observables.

$\Delta x F_3$ is one of the cleaner measurements of CSV in terms of associated experimental systematic uncertainties as this measurement can be extracted from a single target. The challenge here will be to maximize the event samples.

The measurement of ΔF_2 is more complicated as this must combine measurements from both CC and NC experiments which introduces nuclear correction factors. Since NuSOnG will provide high statistics F_2^{CC}measurements for a variety of A targets, this will yield an alternate handle on the CSV and also improve our understanding of the associated nuclear corrections.

The combination of these measurements, together with external constraints, will yield important information on this fundamental symmetry.

VII. DIRECT SEARCHES FOR NEW PHYSICS AT NUSONG

Direct searches for Beyond Standard Model Physics in the NuSOnG detector complement the indirect search for new physics at the Terascale and higher. These studies explore possible low energy manifestations of BSM physics. The searches fall into three broad categories. The first are the searches for new light neutrino properties which include evidence for non-unitarity of the three neutrino mixing matrix. The second are the searches for new interactions manifested through rare events. In particular, NuSOnG is uniquely capable of searching for inverse muon decay in antineutrino mode, which is forbidden in the Standard Model. The third are searches for

new particles observed through decays in the regions between the detector subsections. This includes searches for light neutrissimos, which are moderately-heavy neutral-heavy-leptons ($\sim$ 10 keV to $\sim$ 100 GeV). Searches for axion-like particles, dilaton-like particles, light vector bosons, light inflatons, light radions, etc. which appear in models for BSM physics, are also possible.

In order to focus this discussion, we have selected one example from each category out of the broad palette of possibilities. These examples were chosen for their connection to the previous discussions in this paper and because they address questions about BSM physics which are being actively debated at present. These examples also highlight the unique discovery potential of NuSOnG.

A. Light Neutrino Properties: Matrix Freedom

At this point, it is well established that neutrinos have properties which are not predicted in the Standard Model. Evidence for three light neutrino masses has now been demonstrated through neutrino oscillations in solar, atmospheric, and reactor experiments (see references [124] through [138]). The effect of oscillations requires mixing between the neutrino species. Furthermore, although the MiniBooNE experiment recently refuted the LSND two-neutrino oscillation scenario at $\Delta m^2 \sim 1$ eV^2 [139], the question of the existence of multiple light sterile neutrinos still remains open [140].

These observations already require BSM physics, and consequently raise phenomenological questions, such as: what are the mass and mixing parameters still allowed in sterile neutrino models? What do sterile neutrinos imply about neutrino mixing? Is the neutrino mixing matrix unitary, or is there effective freedom of mixing parameters? These are some of the questions that NuSOnG can potentially address.

An interesting study of light neutrino properties which can be performed at NuSOnG is the search for evidence of "matrix freedom" or "nonunitarity." In this case, the 3×3 matrix describing the three active (SM) neutrinos is not unitary; or, equivalently, the three flavor eigenstates are non-orthogonal (the 3×3 neutrino mixing matrix is *free*) [141]. Nonunitarity can arise in a number of ways. Flavor-dependent neutrino couplings, discussed earlier in this paper, would manifest as nonunitarity. This is because a single coupling is factored out of the contributions to the Lagrangian, and so nonuniversality gets absorbed into the mixing matrix elements. Another example source is the mixing of heavy ($>$ 100 eV), mostly sterile neutrinos (neutrissimos) with light neutrinos. Indeed, the existence of sterile neutrinos at any scale will introduce nonunitarity, simply because the 3×3 mixing matrix is incomplete. Thus one can see that a search for nonunitarity provides a very general test of BSM physics which affects the light neutrino sector.

The constraints on unitarity arise from neutrino oscillations, rare decays and decays of the Z-boson observed at LEP. Which constraints should be applied depend on the model for the cause of non-unitarity. For example, invisible decays of the Z-boson provide no constraint on the apparent nonunitarity caused by introducing sterile neutrinos as long as these weigh less than 40 GeV or so. The most stringent constraints come from new physics which affects rare decays [142].

Nonunitarity introduces striking changes to the probability formula for neutrino flavor transitions, as discussed in reference [142]. Assuming unitarity, the survival probability formula for a neutrino produced as flavor α is

$$P_{\alpha\alpha}^{unitary} = 1 - 4|U_{\alpha 3}|^2[1 - |U_{\alpha 3}|^2] \sin^2 \Delta_{31}, \qquad (89)$$

where one has made use of $\Delta_{31} = \Delta m^2_{31} \frac{L}{4E}$, and $\Delta m^2_{21} \frac{L}{4E} \ll 1$. In the case of matrix freedom, the mixing matrix is no longer unitary. The level at which unitarity is violated can be defined as X_α, where

$$\sum_j |U_{\alpha j}|^2 = 1 - X_\alpha, \qquad (90)$$

with X_α being small. Under that assumption, the survival probability formula is then found to be

$$P_{\alpha\alpha}^{general} = P_{\alpha\alpha}^{unitary} - 2X_\alpha[1 - 2|U_{\alpha 3}|^2 \sin^2 \Delta_{31}] + X_\alpha^2. \qquad (91)$$

To be clear, $P_{\alpha\alpha}^{unitary}$ is the form of Eq. (89) but the sums of the rows and columns of the mixing matrix elements will not add to one in the nonunitary case. From Eq. (91), one important consequence of such scenario is instantaneous (L =0) flavor disappearance in a neutrino beam. A recent study [142] suggests that current experimental data limit such an effect to up to the order of a few percent.

It can be shown that in the case of appearance, matrix freedom leads to a similar instantaneous transition, this time between the active flavors [141] and we can use this signature to search for non-unitarity in NuSOnG. When U is not unitary, then we can define

$$UU^\dagger \equiv \rho. \qquad (92)$$

Then the probability for a transition between flavors α and β is given by

$$P_{\alpha\beta}^{general} = P_{\alpha\beta}^{unitary} - (|\rho_{\alpha\beta}|^2 - \delta_{\alpha\beta}) \qquad (93)$$

The standard oscillation formula for the unitary case is, again, modified by an overall constant. This results in an instantaneous transition at $L = 0$ from ν_α to ν_β [141]. Thus one could observe an excess of ν_e events in a pure ν_μ beam. The excess will have the same energy dependence as the ν_μ flux.

The trick to searching for this instantaneous transition is to focus on an energy range where the ν_e background is low and well constrained. In the case of NuSOnG, this is on the high energy tail of the flux, above E$\gtrsim$ 250 GeV. Using this method, NuSOnG can search for transitions at the $\sim 10^{-5}$ level.

B. New Interactions: Lepton Flavor Violation Searches

The NuSOnG experiment possesses two valuable characteristics for the search for lepton flavor number violation. First, it relies upon a high purity, high intensity beam as its source of neutrinos; secondly, it employs an instrumented detector optimized to measure inverse muon decay with high accuracy. An experiment with these two features naturally lends itself to searches for the process:

$$\bar{\nu}_\mu + e^- \rightarrow \mu^- + \bar{\nu}_e. \tag{94}$$

This interaction is forbidden by the Standard Model with massless neutrinos since it violates lepton flavor number conversion ($\Delta L_e = -\Delta L_\mu = 2$). Furthermore, neutrino mass models that do not predict the existence of other light degrees of freedom (with masses below a TeV or so) lead to unobservably small rates for WSIMD (Eq. (94)), which is best characterized as a flavor changing neutral current phenomenon. Hence, observation of this reaction would immediately constitute direct observation of new weak scale (or below) physics, and may help shed light on the origin of neutrino masses. WSIMD can also be mediated by lepton-number violating interactions (when lepton number is violated $1+(-1)$ times). Theories which incorporate multiplicative lepton number conservation [143, 144], left-right symmetry [145], or the existence of bileptons [146] fall under this category.

It is typical to compare this process to that of inverse muon decay:

$$\sigma_{\bar{\nu}_\mu e^- \rightarrow \mu^- \bar{\nu}_e} = \lambda \frac{G_F^2 s (1-r)^2}{\pi} \left(A_V (\frac{1+r/2}{3}) + A_S \right). \tag{95}$$

Here, G_F the Fermi constant, s the square of the center of mass energy of the system, and r defined as m_μ^2/s. The parameters λ, A_V, and A_S describe the strength of the reaction and whether the process is vector/axial-vector or scalar/pseudo-scalar in nature.

The signature for such a reaction is the tagging of a μ^- during antineutrino running with the same signature as expected from inverse muon decays. The main backgrounds to this reaction include (a) ν_μ contamination ($\nu_\mu + e^- \rightarrow \nu_e + \mu^-$), (b) $\bar{\nu}_e$ contamination ($\bar{\nu}_e + e^- \rightarrow \bar{\nu}_\mu + \mu^-$) and (c) charge misidentification of candidate muons. Our current estimates place a very small beam contamination during antineutrino running: about 0.4% contamination of ν_μs and a 2.3% contamination of ν_e and $\bar{\nu}_e$ neutrinos (See Sec. II). Charge misidentification is expected to be very small, on the order of 10^{-5}. If we assume a conservative knowledge of the backgrounds at the 5% level, this would imply a limit the ratio of WSIMD in $\bar{\nu}$ mode to IMD in ν mode of 0.2%, which leads to a lepton flavor violation cross-section ratio of better than 0.6% (at 90% C.L.) for V-A couplings and less than 0.2% for scalar couplings. Previous searches, based on 1.6×10^{18} protons on target and smaller target masses, have placed limits on this cross-section ratio to less than 1.7% at 90% C.L. for V-A couplings and less than 0.6% for scalar couplings [147]. The NuSOnG experiment can therefore provide a considerable improvement compared to previous searches. This limit can be greatly improved if further selection criteria are used in removing unwanted beam impurities or the wrong-sign background contamination.

Note that the experimental signature for WSIMD is identical to the signature for instantaneous transition due to matrix freedom discussed in the previous section and due to the fact that we are unable to tag the flavor of the outgoing neutrino. In other words $\bar{\nu}_\mu + e^- \rightarrow \mu^- + \bar{\nu}_e$ is indistinguishable from $\bar{\nu}_\mu \rightarrow \bar{\nu}_e$ which then interacts via $\bar{\nu}_e + e^- \rightarrow \mu^- + \bar{\nu}_\mu$. If a beyond standard model signal is observed in this mode and also in the appearance search described above, this would be striking confirmation of non-unitarity. Considering only statistical errors, the limit which could be set on nonunitarity through this study is 1.8×10^{-3}. If an effect is seen in this search and the appearance search described in the previous section, this would provide powerful evidence for matrix freedom.

C. New Particles: Long-lived, Very Low Mass Neutrissimos

While this paper has largely focussed on TeV-scale physics, where heavy neutrissimos may appear, it is also possible that light neutrissimos (N) with masses as low as a few keV, exist. An example of a phenomenological model which motivates light neutrissimos can be found in refs. [148] and [149] (see also [150, 151]), where in the latter it is referred to as the νMSM (neutrino Minimal Standard Model). These models incorporate neutrino mass by extending the lepton sector such that every left-handed fermion has a right-handed partner (so it is introducing three neutrino partners). A nice aspect of the νMSM model is that it may provide a dark matter candidate in the form of a few keV neutrissimo, and it has a mechanism for the baryon asymmetry in the universe if the two other masses are larger (> 100 MeV), nearly degenerate and with tiny mixings [152, 153]. Such a pattern can be nicely justified by evoking lepton number symmetries which are slightly broken. The predicted mass range for neutrissimos in the νMSM model is 2 keV$< m_N < 5$ GeV.

Experimental motivation for this search may arise from LHC results and be motivated by NuTeV observations. If an ~ 100 GeV neutrissimo is observed at LHC, then a search for a lower mass neutrissimo is well motivated. Such an observation would imply a complex and interesting neutrissimo sector [154, 155].

Another motivation arises from a NuTeV search for long-lived, light (< 15 GeV) neutral heavy leptons. This was performed in a helium-filled decay region located up-

stream of the calorimeter. In the mass region of 2.2-15 GeV, NuTeV has a small expected background (0.07 ± 0.01 events), but observed three events. All events had two muons originating from a vertex within the helium decay region and missing energy [156]. Since publication in 2001, no widely accepted explanation has been found. In 2006, D0 published a search for a similar decay signature in proton-antiproton interactions [157]. No events were found and some production models were excluded. The most viable remaining model [158] hypothesizes that the events are from decay of long-lived neutralinos produced in the NuTeV beam dump through B hadron decays. No other experiment has been able to match NuTeV's running conditions to further explore this result.

NuSOnG can address the question by including a low-mass (helium-filled) decay region between the calorimeter segments. Assuming parameters similar to those of NuTeV (except for a 20-fold increase in the number of protons on target), NuSOnG would expect to see 60 events with an expected background of 1-2 events. The sensitivity would scale directly with the decay volume, so the increased length compared to NuTeV ($26\ m \rightarrow \approx 40\ m$) would increase this to 90 signal events over a 2-3 event background. Observing no signal would finally settle this outstanding question.

These decay regions allow exploration for a signal from a BSM particle in other decay modes as well; other interesting modes include $\mu\pi$, μe, $e\pi$ and ee. In particular, the NuSOnG detector is optimized for observation of decays to electrons, unlike NuTeV which had 4 inch steel plates between the detectors in the calorimeter. NuSOnG's sensitivity to other new particles is also improved over NuTeV by the increase in beam intensity and decay volume, allowing us to study new regions of phase space. The NuSOnG decay region is very versatile and searches for other particles, beyond neutrissimos, as described in the introduction to this section, can also be accomplished.

VIII. SUMMARY AND CONCLUSIONS

NuSOnG is an experiment which can search for new physics from keV through TeV energy scales. This article has focussed mainly on the Terascale physics which can be accessed through this new high energy, high statistics neutrino scattering experiment. The case has been made that this new neutrino experiment would be a valuable addition to the presently planned suite of experiments with Terascale reach.

The NuSOnG experiment design draws on the heritage of the CHARM II and CCFR/NuTeV experiments. A high energy, flavor-pure neutrino flux is produced using 800 GeV protons from the Tevatron. The detector consists of four modules, each composed of a finely-segmented glass-target (SiO_2) calorimeter followed by a muon spectrometer. In its five-year data acquisition period, this experiment will record almost one hundred thousand neutrino-electron elastic scatters and hundreds of millions of deep inelastic scattering events, exceeding the current world data sample by more than an order of magnitude. This experiment can address concerns related to model systematics of electroweak measurements in neutrino-quark scattering by direct constraints using *in-situ* structure function measurements.

NuSOnG will be unique among present and planned experiments for its ability to probe neutrino couplings to Beyond Standard Model physics. This experiment offers four distinct and complementary probes of S and T. Two are of high precision with the proposed run-plan, and the precision of the other two would be improved by a follow-up five-year antineutrino run. Neutrino-lepton non-standard interactions can be probed with an order of magnitude improvement in the measured effective couplings. Neutrino-quark non-standard interactions can be probed by an improvement in the measured neutrino-quark effective couplings of a factor of two or better. The experiment is sensitive to new physics up to energy scales ~ 5 TeV at 95% CL. The measurements are sensitive to universality of the couplings and an improvement in the e-family of 30% and μ-family of 75% will allow for probes of neutrissimos. As a unique contribution, NuSOnG measures g_R/g_L, which is not accessible by other near-future experiments. This article described NuSOnG's physics contribution under several specific models. These included models of Z's, extended Higgs models, leptoquark models and R-parity violating SUSY models. We also considered how, once data are taken at LHC and NuSOnG, the underlying physics can be extracted. The opportunity for direct searches related to these indirect electroweak searches was also described. The conclusion of our analysis is that a new neutrino experiment, such as NuSOnG, would substantially enhance the presently planned Terascale program.

Acknowledgments

We thank the following people for their thoughtful comments on the development of this physics case: P. Langacker, M. Shaposhnikov, F. Vannucci, J. Wells.

We acknowledge the support of the following funding agencies for the authors of this paper: Deutsche Forschungsgemeinschaft, The Kavli Institute for Theoretical Physics, The United States Department of Energy, The United States National Science Foundation.

[1] The NuSOnG Expression of Interest is available from the Fermilab Directorate or at http://www-nusong.fnal.gov

[2] C. A. Gagliardi, R. E. Tribble and N. J. Williams, Phys. Rev. D **72** (2005) 073002 [arXiv:hep-ph/0509069]; A. Gaponenko *et al.* [TWIST Collaboration], Phys. Rev. D **71** (2005) 071101 [arXiv:hep-ex/0410045]; A. Gaponenko *et al.* [TWIST Collaboration], Phys. Rev. D **71** (2005) 071101 [arXiv:hep-ex/0410045].

[3] L. A. Ahrens *et al.*, Phys. Rev. D **41**, 3297 (1990).

[4] P. Vilain *et al.*, Phys. Lett. B335: 246, 1994.

[5] E. A. Paschos and L. Wolfenstein, Phys. Rev. D **7**, 91 (1973).

[6] R. Bernstein et al.; "Sign-Selected Quadrupole Train"; FERMILAB-TM-1884, April 1994; J. Yu et al.; "NuTeV SSQT Performance"; FERMILAB-TM-2040,February 1998.

[7] Fermilab Beams Division Public Documents numbers 2222, 2849; accessible at: http://beamdocs.fnal.gov/AD-public/DocDB/ShowDocument?docid=2222; http://beamdocs.fnal.gov/AD-public/DocDB/ShowDocument?docid=2849

[8] D. Geiregat *et al.* [CHARM-II Collaboration], Nucl. Instrum. Meth. A **325**, 92 (1993). K. De Winter *et al.* [CHARM-II Collaboration], Nucl. Instrum. Meth. A **278**, 670 (1989); K. De Winter *et al.* [CHARM-II Collaboration], Nucl. Instrum. Meth. A **277**, 83 (1989).

[9] G. P. Zeller, "A precise measurement of the weak mixing angle in neutrino nucleon scattering," (Thesis) UMI-30-50615

[10] G. Barichello *et al.*, Nucl. Instrum. Meth. A **506**, 217 (2003); M. Ellis and F. J. P. Soler, J. Phys. G **29**, 1975 (2003).

[11] W.-M. Yao et al., J. Phys. **G 33**, 1, (2006)

[12] M. Tzanov *et al.*, Phys. Rev. D **74**012008, 2006.

[13] W. J. Marciano and Z. Parsa, J. Phys. G **29**, 2629 (2003) [arXiv:hep-ph/0403168].

[14] S. Sarantakos, A. Sirlin and W. J. Marciano, Nucl. Phys. B **217**, 84 (1983).

[15] U. Baur, private communication.

[16] D. Drakoulakos *et al.* [Minerva Collaboration], "Proposal to perform a high-statistics neutrino scattering experiment using a fine-grained detector in the NuMI beam," arXiv:hep-ex/0405002.

[17] See presentations at: http://www.fnal.gov/directorate/Longrange/Steering_Public/workshop-physics.html.

[18] Nucl. Instrum. Meth. A **447**, 377 (2000) [arXiv:hep-ex/9908056].

[19] D. Casper, Nucl. Phys. Proc. Suppl. **112**, 161 (2002).

[20] D. Puseljic, *et al.*, IEEE Trans. on Nuc. Sci., 35:1, 475, 1988; D.E. Wagoner, *et al.* IEEE Trans. on Nuc. Sci. **31:1**, 53, 1984;

[21] S. E. Avvakumov, "Search for mu/nu (anti-mu/nu) –¿ nu/e (anti-nu/e) oscillations in the E815 (NuTeV) fixed target neutrino experiment at Fermilab," (Thesis) UMI-30-35594.

[22] A. Pla-Dalmau, A. D. Bross, V. V. Rykalin and B. M. Wood [MINERvA Collaboration], "Extruded plastic scintillator for MINERvA," FERMILAB-CONF-05-506-E; P. Adamson *et al.* [MINOS Collaboration], IEEE Trans. Nucl. Sci. **49**, 861 (2002).

[23] S. Alekhin, S. A. Kulagin and R. Petti, AIP Conf. Proc. **967**, 215 (2007) [arXiv:0710.0124 [hep-ph]]; G. Onengut *et al.* [CHORUS Collaboration], Phys. Lett. B **632**, 65 (2006).

[24] G. P. Zeller *et al.* Phys. Rev. Lett., **88** 091802, 2002.

[25] S. C. Bennett and Carl E. Wieman, Phys. Rev. Lett., **82** 2484–2487, 1999.

[26] P. L. Anthony *et al.* [SLAC E158 Collaboration], Phys. Rev. Lett. **95**, 081601 (2005) [arXiv:hep-ex/0504049].

[27] http://www.slac.stanford.edu/exp/e158/

[28] A. Sher *et al.*, Phys. Rev. Lett. **91**, 261802 (2003) [arXiv:hep-ex/0305042].

[29] V. Cirigliano, H. Neufeld and H. Pichl, Eur. Phys. J. C **35**, 53 (2004) [arXiv:hep-ph/0401173].

[30] J. R. Batley *et al.* [NA48/2 Collaboration], Eur. Phys. J. C **50**, 329 (2007) [Erratum-ibid. C **52**, 1021 (2007)] [arXiv:hep-ex/0702015].

[31] G.P. Zeller, private communication.

[32] D. A. Mason, "Measurement of the strange - antistrange asymmetry at NLO in QCD from NuTeV dimuon data," Phys. Rev. Lett. **99**, 192001 (2007).

[33] K. P. O. Diener, S. Dittmaier, and W. Hollik, Phys. Rev. D **69**, 073005 (2004) [arXiv:hep-ph/0310364].

[34] B. A. Dobrescu and R. K. Ellis, Phys. Rev. D **69**, 114014 (2004) [arXiv:hep-ph/0310154].

[35] S. Moch, M. Rogal and A. Vogt, Nucl. Phys. B **790**, 317 (2008) [arXiv:0708.3731 [hep-ph]].

[36] I. Schienbein *et al.*, accepted to J. Phys. G: Nucl. Part. Phys., arXiv:0709.1775 [hep-ph].

[37] K. S. McFarland and S. O. Moch, arXiv:hep-ph/0306052; S. Kretzer and M. H. Reno, Phys. Rev. D **69**, 034002 (2004) [arXiv:hep-ph/0307023].

[38] M. Gluck, P. Jimenez-Delgado, and E. Reya, arXiv:hep-ph/0501169; F. M. Steffens and K. Tsushima, Phys. Rev. D **70**, 094040 (2004) [arXiv:hep-ph/0408018]; J. T. Londergan and A. W. Thomas, arXiv:hep-ph/0407247; A. D. Martin, R. G. Roberts, W. J. Stirling, and R. S. Thorne, Eur. Phys. J. C **39**, 155 (2005) [arXiv:hep-ph/0411040].

[39] M. E. Peskin and T. Takeuchi, Phys. Rev. D **46**, 381 (1992).

[40] M. E. Peskin and T. Takeuchi, Phys. Rev. Lett. **65**, 964 (1990).

[41] M. E. Peskin and J. D. Wells, Phys. Rev. D **64**, 093003 (2001) [arXiv:hep-ph/0101342].

[42] Z. Berezhiani, R. S. Raghavan and A. Rossi, Nucl. Phys. B **638**, 62 (2002) [arXiv:hep-ph/0111138].

[43] A. Bandyopadhyay *et al.* [ISS Physics Working Group], arXiv:0710.4947 [hep-ph].

[44] J. Barranco, O. G. Miranda, C. A. Moura and J. W. F. Valle, arXiv:0711.0698 [hep-ph].

[45] W. Loinaz, N. Okamura, S. Rayyan, T. Takeuchi and L. C. R. Wijewardhana, Phys. Rev. D **68**, 073001 (2003) [arXiv:hep-ph/0304004].

[46] W. Loinaz, N. Okamura, S. Rayyan, T. Takeuchi and L. C. R. Wijewardhana, Phys. Rev. D **70**, 113004 (2004) [arXiv:hep-ph/0403306].

[47] S. Davidson, C. Pena-Garay, N. Rius and A. Santamaria, JHEP **0303**, 011 (2003) [arXiv:hep-ph/0302093].

[48] R. N. Mohapatra *et al.*, Rept. Prog. Phys. **70**, 1757 (2007) [arXiv:hep-ph/0510213].

[49] M. Carena, A. de Gouvêa, A. Freitas, and M. Schmitt, Phys. Rev. D **68**, 113007 (2003) [arXiv:hep-ph/0308053].

[50] ElectroWeak Working Group, ALEPH, DELPI, L3, OPAL, and SLD Collaborations, arXiv:hep-ex/0212036.

[51] A. de Gouvêa and J. Jenkins, Phys. Rev. D **74**, 033004 (2006) [arXiv:hep-ph/0603036].

[52] P. Langacker, arXiv:0801.1345 [hep-ph].

[53] M. S. Carena, A. Daleo, B. A. Dobrescu and T. M. P. Tait, Phys. Rev. D **70**, 093009 (2004) [arXiv:hep-ph/0408098].

[54] X. G. He, G. C. Joshi, H. Lew and R. R. Volkas, Phys. Rev. D **43**, R22 (1991);
X. G. He, G. C. Joshi, H. Lew and R. R. Volkas, Phys. Rev. D **44**, 2118 (1991).

[55] S. Baek, N. G. Deshpande, X. G. He and P. Ko, Phys. Rev. D **64**, 055006 (2001) [arXiv:hep-ph/0104141];
E. Ma, D. P. Roy and S. Roy, Phys. Lett. B **525**, 101 (2002) [arXiv:hep-ph/0110146]; S. Choubey and W. Rodejohann, Eur. Phys. J. C **40**, 259 (2005) [arXiv:hep-ph/0411190];
W. Rodejohann and M. A. Schmidt, Phys. Atom. Nucl. **69**, 1833 (2006) [arXiv:hep-ph/0507300];
B. Adhikary, Phys. Rev. D **74**, 033002 (2006) [arXiv:hep-ph/0604009];
T. Ota and W. Rodejohann, Phys. Lett. B **639**, 322 (2006) [arXiv:hep-ph/0605231];
E. J. Chun and K. Turzynski, arXiv:hep-ph/0703070.

[56] E. Ma, Phys. Lett. B **433**, 74 (1998) [arXiv:hep-ph/9709474];
E. Ma and D. P. Roy, Phys. Rev. D **58**, 095005 (1998) [arXiv:hep-ph/9806210];
E. Ma and U. Sarkar, Phys. Lett. B **439**, 95 (1998) [arXiv:hep-ph/9807307];
L. N. Chang, O. Lebedev, W. Loinaz, and T. Takeuchi, Phys. Rev. D **63**, 074013 (2001) [arXiv:hep-ph/0010118];
P. B. Pal and U. Sarkar, Phys. Lett. B **573**, 147 (2003) [arXiv:hep-ph/0306088].

[57] E. Ma, D. P. Roy and U. Sarkar, Phys. Lett. B **444**, 391 (1998) [arXiv:hep-ph/9810309].

[58] E. Ma and D. P. Roy, Phys. Rev. D **59**, 097702 (1999); [arXiv:hep-ph/9811266].

[59] E. Ma and D. P. Roy, arXiv:hep-ph/0111385.

[60] S. Davidson, S. Forte, P. Gambino, N. Rius and A. Strumia, JHEP **0202**, 037 (2002) [arXiv:hep-ph/0112302].

[61] A. Zee, Phys. Lett. B **93**, 389 (1980) [Erratum-ibid. B **95**, 461 (1980)].

[62] K. S. Babu, Phys. Lett. B **203**, 132 (1988);
A. Zee, Nucl. Phys. B **264**, 99 (1986).

[63] L. J. Hall and M. Suzuki, Nucl. Phys. B **231**, 419 (1984);
H. E. Haber and G. L. Kane, Phys. Rept. **117**, 75 (1985);
M. Nowakowski and A. Pilaftsis, Nucl. Phys. B **461**, 19 (1996) [arXiv:hep-ph/9508271];
S. P. Martin, arXiv:hep-ph/9709356.

[64] R. Barbier *et al.*, Phys. Rept. **420**, 1 (2005) [arXiv:hep-ph/0406039].

[65] W. Buchmuller, R. Ruckl and D. Wyler, Phys. Lett. B **191**, 442 (1987) [Erratum-ibid. B **448**, 320 (1999)].

[66] J. Blumlein and R. Ruckl, Phys. Lett. B **304**, 337 (1993);
M. Tanabashi, in the Review of Particle Physics [70].

[67] S. Davidson, D. C. Bailey and B. A. Campbell, Z. Phys. C **61**, 613 (1994) [arXiv:hep-ph/9309310].

[68] M. Honda, Y. Kao, N. Okamura, A. Pronin and T. Takeuchi, arXiv:0707.4545 [hep-ph].

[69] W. Loinaz, A. Pronin, T. Takeuchi, in preparation.

[70] W. M. Yao *et al.* [Particle Data Group], J. Phys. G **33**, 1 (2006).

[71] M. E. Peskin and T. Takeuchi, Phys. Rev. D **46**, 381 (1992).

[72] J. L. Rosner, Phys. Rev. D **70**, 037301 (2004) arXiv:hep-ph/0404264.

[73] M. E. Peskin and J. D. Wells, Phys. Rev. D **64**, 093003 (2001) [arXiv:hep-ph/0101342].

[74] T. Takeuchi and W. Loinaz, arXiv:hep-ph/0410201.

[75] A. Belyaev, C. Leroy, R. Mehdiyev and A. Pukhov, JHEP **0509**, 005 (2005) [arXiv:hep-ph/0502067].

[76] E. Gabrielli, Phys. Rev. D **62**, 055009 (2000) [arXiv:hep-ph/9911539];

[77] S. Davidson, S. Forte, P. Gambino, N. Rius, and A. Strumia, JHEP **0202**, 037 (2002) [arXiv:hep-ph/0112302].

[78] G. D. Kribs, T. Plehn, M. Spannowsky, and T. M. P. Tait, arXiv:0706.3718 [hep-ph].

[79] W.G. Seligman, Ph. D. Thesis, Nevis Report 292.

[80] M. Shaevitz, Private Communication.

[81] M. Arneodo *et al.* [New Muon Collaboration], Nucl. Phys. B **483**, 3 (1997) [arXiv:hep-ph/9610231].

[82] U. K. Yang *et al.* [CCFR/NuTeV Collaboration], Phys. Rev. Lett. **87**, 251802 (2001) [arXiv:hep-ex/0104040].

[83] CCFR Collaboration: W. G. Seligman *et al.*, Phys. Rev. Lett **79**12131997 [hep-ex/970107]; CCFR Collaboration: U. K. Yang *et al.*, Phys. Rev. Lett **86**27422001 [hep-ex/0009041].

[84] U. K. Yang *et al.* [CCFR/NuTeV Collaboration], arXiv:hep-ex/9806023.

[85] C. K. McNulty, Ph. D. Thesis, UMI-98-09743.

[86] S.A. Kulagin and R. Petti, Nuc. Phys. **A765**,126,2006.

[87] S. J. Brodsky, I. Schmidt and J. J. Yang, Phys. Rev. D **70**, 116003 (2004) [arXiv:hep-ph/0409279].

[88] I. Schienbein, J. Y. Yu, C. Keppel, J. G. Morfin, F. Olness and J. F. Owens, arXiv:0710.4897 [hep-ph].

[89] The Impact of New Neutrino DIS and Drell-Yan Data J.F. Owens *et al.*, Phys. Rev. **D75**,054030, 2007 [hep-ph/0702159].

[90] A. O. Bazarko *et al.* [CCFR Collaboration], Z. Phys. C **65**, 189 (1995) [arXiv:hep-ex/9406007].

[91] M. Goncharov *et al.* [NuTeV Collaboration], Phys. Rev. D **64**, 112006 (2001) [arXiv:hep-ex/0102049].

[92] M. Tzanov *et al.* [NuTeV Collaboration], arXiv:hep-ex/0306035.

[93] P. Vilain *et al.* [CHARM II Collaboration], Eur. Phys. J. C **11**, 19 (1999).

[94] P. Astier *et al.* [NOMAD Collaboration], Phys. Lett. B **486**, 35 (2000).

[95] G. P. Zeller *et al.* [NuTeV Collaboration], Phys. Rev. D **65**, 111103 (2002) [Erratum-ibid. D **67**, 119902 (2003)] [arXiv:hep-ex/0203004].

[96] V. Barone, C. Pascaud, and F. Zomer, Eur. Phys. J. C **12**, 243 (2000) [arXiv:hep-ph/9907512].

[97] K. S. McFarland and S. O. Moch, arXiv:hep-ph/0306052.

[98] F. Olness *et al.*, Eur. Phys. J. C **40**, 145 (2005)

[arXiv:hep-ph/0312323].
[99] A. O. Bazarko *et al.* [CCFR Collaboration], Z. Phys. C **65**, 189 (1995) [arXiv:hep-ex/9406007]; S. A. Rabinowitz *et al.*, Phys. Rev. Lett. **70**, 134 (1993).
[100] A. Kayis-Topaksu *et al.* [CHORUS Collaboration], Phys. Lett. B **549**, 48 (2002).
[101] P. Astier *et al.* [NOMAD Collaboration], Phys. Lett. B **486**, 35 (2000).
[102] T. Bolton, 'Determining the CKM parameter V(cd) from nu N charm production," (1997) arXiv:hep-ex/9708014;
[103] P. Vilain *et al.* [CHARM II Collaboration], Eur. Phys. J. C **11**, 19 (1999).
[104] H. Abramowicz *et al.*, Z. Phys. C **15**, 19 (1982).
[105] P. H. Sandler *et al.*, Phys. Rev. D **42**, 759 (1990).
[106] P. H. Sandler *et al.*, Z. Phys. C **57**, 1 (1993).
[107] P. H. Sandler, Ph. D. Thesis, UMI-92-18364-MC.
[108] C. Boros, F. M. Steffens, J. T. Londergan and A. W. Thomas, Phys. Lett. B **468**, 161 (1999) [arXiv:hep-ph/9908280].
[109] R. D. Ball, D. A. Harris and K. S. McFarland, arXiv:hep-ph/0009223.
[110] S. Kretzer, F. I. Olness, R. J. Scalise, R. S. Thorne and U. K. Yang, Phys. Rev. D **64**, 033003 (2001) [arXiv:hep-ph/0101088].
[111] A. D. Martin, R. G. Roberts, W. J. Stirling and R. S. Thorne, Eur. Phys. J. C **23**, 73 (2002) [arXiv:hep-ph/0110215].
[112] C. Boros, J. T. Londergan and A. W. Thomas, Phys. Rev. D **59**, 074021 (1999) [arXiv:hep-ph/9810220].
[113] C. Boros, J. T. Londergan and A. W. Thomas, Phys. Rev. Lett. **81**, 4075 (1998) [arXiv:hep-ph/9806249].
[114] A. Baldit *et al.* [NA51 Collaboration], Phys. Lett. B **332**, 244 (1994).
[115] A. D. Martin, R. G. Roberts, W. J. Stirling and R. S. Thorne, Eur. Phys. J. C **39**, 155 (2005) [arXiv:hep-ph/0411040].
[116] M. Roth and S. Weinzierl, Phys. Lett. B **590**, 190 (2004) [arXiv:hep-ph/0403200].
[117] M. Gluck, P. Jimenez-Delgado and E. Reya, Phys. Rev. Lett. **95**, 022002 (2005) [arXiv:hep-ph/0503103].
[118] F. Abe *et al.* [CDF Collaboration], Phys. Rev. Lett. **81**, 5754 (1998) [arXiv:hep-ex/9809001].
[119] A. Bodek, Q. Fan, M. Lancaster, K. S. McFarland and U. K. Yang, Phys. Rev. Lett. **83**, 2892 (1999) [arXiv:hep-ex/9904022].
[120] J. F. Owens *et al.*, Phys. Rev. D **75**, 054030 (2007) [arXiv:hep-ph/0702159].
[121] J. Pumplin, D. R. Stump, J. Huston, H. L. Lai, P. Nadolsky and W. K. Tung, JHEP **0207**, 012 (2002) [arXiv:hep-ph/0201195].
[122] D. Allasia *et al.* [New Muon Collaboration (NMC)], Phys. Lett. B **249**, 366 (1990).
[123] E. A. Hawker *et al.* [FNAL E866/NuSea Collaboration], Phys. Rev. Lett. **80**, 3715 (1998) [arXiv:hep-ex/9803011].
[124] B. T. Cleveland *et al.*, Astrophys. J. **496**, 505 (1998).
[125] Y. Fukuda *et al.* [Super-Kamiokande Collaboration], Phys. Rev. Lett. **81**, 1158 (1998) [Erratum-ibid. **81**, 4279 (1998)] [arXiv:hep-ex/9805021]; Phys. Rev. Lett. **82**, 2430 (1999) [arXiv:hep-ex/9812011].
[126] J. N. Abdurashitov *et al.* [SAGE Collaboration], J. Exp. Theor. Phys. **95**, 181 (2002) [Zh. Eksp. Teor. Fiz. **122**, 211 (2002)] [arXiv:astro-ph/0204245].
[127] W. Hampel *et al.* [GALLEX Collaboration], Phys. Lett. B **447**, 127 (1999).
[128] M. Altmann *et al.* [GNO Collaboration], Phys. Lett. B **490**, 16 (2000) [arXiv:hep-ex/0006034].
[129] Q. R. Ahmad *et al.* [SNO Collaboration], Phys. Rev. Lett. **89**, 011301 (2002) [arXiv:nucl-ex/0204008]; Phys. Rev. Lett. **89**, 011302 (2002) [arXiv:nucl-ex/0204009]; Phys. Rev. Lett. **87**, 071301 (2001) [arXiv:nucl-ex/0106015].
[130] T. Araki *et al.* [KamLAND Collaboration], Phys. Rev. Lett. **94**, 081801 (2005) [arXiv:hep-ex/0406035].
[131] Y. Fukuda *et al.* [Super-Kamiokande Collaboration], Phys. Lett. B **433**, 9 (1998) [arXiv:hep-ex/9803006]; Phys. Lett. B **436**, 33 (1998) [arXiv:hep-ex/9805006]; Phys. Rev. Lett. **81**, 1562 (1998) [arXiv:hep-ex/9807003]; Phys. Rev. Lett. **82**, 2644 (1999) [arXiv:hep-ex/9812014]; Phys. Lett. B **467**, 185 (1999) [arXiv:hep-ex/9908049]; Y. Ashie *et al.* [Super-Kamiokande Collaboration], Phys. Rev. D **71**, 112005 (2005) [arXiv:hep-ex/0501064].
[132] D. Casper *et al.*, Phys. Rev. Lett. **66**, 2561 (1991); R. Becker-Szendy *et al.*, Phys. Rev. Lett. **69**, 1010 (1992).
[133] M. Ambrosio *et al.* [MACRO Collaboration], Phys. Lett. B **434**, 451 (1998) [arXiv:hep-ex/9807005]; Phys. Lett. B **478**, 5 (2000) [arXiv:hep-ex/0001044]; Phys. Lett. B **517**, 59 (2001) [arXiv:hep-ex/0106049]; Phys. Lett. B **566**, 35 (2003) [arXiv:hep-ex/0304037].
[134] W. W. M. Allison *et al.*, Phys. Lett. B **391**, 491 (1997) [arXiv:hep-ex/9611007]; Phys. Lett. B **449**, 137 (1999) [arXiv:hep-ex/9901024]; M. C. Sanchez *et al.* [Soudan 2 Collaboration], [arXiv:hep-ex/0307069].
[135] S. H. Ahn *et al.* [K2K Collaboration], Phys. Lett. B **511**, 178 (2001) [arXiv:hep-ex/0103001]; Phys. Rev. Lett. **90**, 041801 (2003) [arXiv:hep-ex/0212007]; Phys. Rev. D **74**, 072003 (2006) [arXiv:hep-ex/0606032].
[136] D. G. Michael *et al.* [MINOS Collaboration], [arXiv:hep-ex/0607088].
[137] M. Apollonio *et al.*, Eur. Phys. J. C **27**, 331 (2003) [arXiv:hep-ex/0301017].
[138] T. Araki *et al.* [KamLAND Collaboration], [arXiv:hep-ex/0406035].
[139] A. A. Aguilar-Arevalo *et al.* [The MiniBooNE Collaboration], arXiv:0704.1500 [hep-ex].
[140] M. Maltoni and T. Schwetz, [arXiv:hep-ph/0705.0107].
[141] Boris Kayser, private communication.
[142] S. Antusch *et al.*, [arXiv:hep-ph/0607020].
[143] G. Feinberg and S. Weinberg, Phys. Rev. Lett. **6**, 381 (1961)
[144] A. Ibarra, E. Masso, and J. Redondo, Nucl. Phys. B **715**, 523 (2005) [arXiv:hep-ph/0410386].
[145] P. Herczeg and R. N. Mohapatra, Phys. Rev. Lett. **69**, 2475 (1992).
[146] S. Godfrey, P. Kalyniak, and N. Romanenko, Phys. Rev. D **65**, 033009 (2002) [arXiv:hep-ph/0108258].
[147] J. A. Formaggio *et al.* [NuTeV Collaboration], Phys. Rev. Lett. **87**, 071803 (2001) [arXiv:hep-ex/0104029].
[148] A. de Gouvêa, Phys. Rev. D **72**, 033005 (2005) [arXiv:hep-ph/0501039].
[149] T. Asaka and M. Shaposhnikov, Phys. Lett. B **620**, 17 (2005) [arXiv:hep-ph/0505013].
[150] A. de Gouvêa, J. Jenkins and N. Vasudevan, Phys. Rev. D **75**, 013003 (2007) [arXiv:hep-ph/0608147].
[151] D. Gorbunov and M. Shaposhnikov, JHEP **0710**, 015

(2007) [arXiv:0705.1729 [hep-ph]].
[152] M. Shaposhnikov, Nucl. Phys. B **763**, 49 (2007) [arXiv:hep-ph/0605047].
[153] D. Gorbunov and M. Shaposhnikov, JHEP **0710**, 015 (2007) [arXiv:0705.1729 [hep-ph]].
[154] A. de Gouvêa, arXiv:0706.1732 [hep-ph].
[155] J. Kersten and A. Y. Smirnov, Phys. Rev. D **76**, 073005 (2007) [arXiv:0705.3221 [hep-ph]].
[156] T. Adams *et al.* [NuTeV Collaboration], Phys. Rev. Lett. **87**, 041801 (2001) [arXiv:hep-ex/0104037].
[157] V. M. Abazov *et al.* [D0 Collaboration], Phys. Rev. Lett. **97**, 161802 (2006) [arXiv:hep-ex/0607028].
[158] A. Dedes, H. K. Dreiner, and P. Richardson, Phys. Rev. D **65**, 015001 (2002) [arXiv:hep-ph/0106199].